AN ABSTRACT OF THE THESIS OF

Louise Hunt for the degree of Master of Science in Oceanography presented on October 18, 2002.

Title: An X-Radiographic Study of the October 2000 Po River Flood Deposit, Italy.

Abstract approved Redacted for privacy

Robert A. Wheatcroft

During October 2000 the Po River, Italy's largest river, experienced a historically significant flood, producing a deposit on the adjacent prodelta. In December 2000 an event-response study of the deposit was conducted, and during the ensuing 16 months three additional sampling cruises were conducted to study the subsequent evolution of the deposit.

X-radiograph analysis techniques were developed to enable objective, quantitative measurements of deposit thickness. Two methods of objectively locating the deposit base were created and verified with a data set of x-radiographs from a previously studied flood deposit.

The Po River flood deposit was found to be proximal to the river mouths with a sharp cross-shore thickness gradient, from 38-cm thick in 11-m water depth off the Pila mouth, to the deposit edge approximately 7 km seaward in 30-m water depth. Along-shore deposit thickness was varied; deposit thickness was high (> 15 cm) at near shore (10-m depth) stations proximal to river mouths and low (7 cm) at other near-shore stations. This distribution was likely a result of the low energy

shelf environment allowing immediate deposition of Po River sediment load with little dispersal or resuspension. The located deposit mass was approximately 10^7 T.

Continued deposition and bioturbation occurred at most sites between December 2000 and June 2001. Sites proximal to the Pila mouth showed continued deposition through April 2002 at rates of up to 15 cm/yr. Between December 2000 and April 2002 no significant erosion occurred; consistent with the generally low velocity bottom currents measured at a benthic tripod in the study area.

An X-Radiographic Study of the October 2000 Po River Flood Deposit, Italy.

by

Louise Hunt

A THESIS

submitted to

Oregon State University

in partial fulfillment of
the requirements for the
degree of

Master of Science

Presented October 18, 2002

Commencement June 2003

Master of Science thesis of Louise Hunt presented on October 18, 2002.

APPROVED:

Redacted for privacy

Major Professor, representing Oceanography

Redacted for privacy

Dean of the College of Oceanic and Atmospheric Sciences

Redacted for privacy

Dean of the Graduate School

I understand that my thesis will become part of the permanent collection of Oregon State University libraries. My signature below authorizes release of my thesis to any reader upon request.

Redacted for privacy

Louise Hunt, Author

ACKNOWLEDGMENTS

First and foremost I would like to thank Rob Wheatcroft, my advisor, for his influence on the past 4 years of my life. To come and work as a research assistant on a project in the Bahamas was a dream. During this time his encouragement to attend graduate school lead me to the decision to stay on in the US and turn a fun 6 months into a valuable, but more importantly enjoyable 4 years. His active interest and ongoing guidance throughout the project and thesis writing provided a steep learning curve that I am grateful to have climbed.

I am grateful to Rob Holman, Clare Reimers, and Mark Christensen for their time, guidance, and interest in this project. And to my lab-mates, Roger Lewis, Cara Fritz, and Andrew Stevens, thanks for all the help and enlightening conversations – work related too. I would like to thank a succession of Matlab gurus that taught me all things Matlab; Soupie Alexander, Chris Chickadel, Larry O'Neill and Andrew Stevens. Many thanks also to Hoa for keeping cool during the project. I appreciate the writing motivation provided by Sue Potter, I would no doubt be in draft phase were the stakes to defend first not so high - I'll take the Normals tofu salad thanks!

Maziet Cheseby has been like family during my time here, providing suggestions with my work each step of the way, as well as a treasured friendship. The group of awesome friends I have made in the past four years here have helped make a foreign place feel like a great home.

Mark Treadwell has been the encouragement behind many a great feat in my life, this being another to add to the list – thanks heaps for your motivation. Also I would like to thank my family and friends back home in New Zealand for their support and patience.

TABLE OF CONTENTS

TABLE OF CONTENTS (continued)

LIST OF FIGURES

LIST OF FIGURES (continued)

LIST OF FIGURES (continued)

LIST OF TABLES

LIST OF APPENDIX TABLES

AN X-RADIOGRAPHIC STUDY OF THE OCTOBER 2000 PO RIVER FLOOD DEPOSIT, ITALY.

INTRODUCTION

Episodic depositional events play a fundamental role in building the sedimentary record (e.g., Dott, 1983; Wheatcroft, 1990; Pemberton and MacEachern, 1997; Wheatcroft and Drake, 2002). Allochthonous sediment, supplied in part by rivers during flooding, may constitute a significant component of shelf strata, such that the majority of the sedimentary record represents episodic or discontinuous events, rather than reflecting day-to-day, steady-state conditions (Dott, 1983; Leithold, 1989). However, large magnitude, short duration events such as floods are difficult to study as they are rare on decadal time scales; hence a rapid-response study approach is needed, which can be difficult to plan antecedently (Wheatcroft and Borgeld, 2000). Nevertheless, studies of episodic flood events have occurred previously. For example, Wheatcroft et al., (1996) document a large-scale study of strata formation on the Eel River margin, northern California, where a flood with an approximate 30-year return period occurred.

In October 2000 a historically significant flood on the Po River (Figure 1), provided an opportunity to conduct a rapid-response study of episodic sedimentation on the prodelta. An initial response cruise was organized, and in operation by the first week of December 2000. Three subsequent cruises in the ensuing 16 months provided a data set from which to study initial distribution and subsequent evolution of the deposit. The low energy environment of the northern Adriatic study site provided contrast to flood deposition on the high energy Eel River margin.

Information about the initial deposition of sedimentary strata is important because it facilitates an understanding of physical properties and environmental processes occurring at the site, and provides a frame of reference for the interpretation of changes in the depositional environment (Axelsson, 1983; Wheatcroft and Borgeld, 2000). Sediment deposition information is necessary for calculating sediment budgets, as well as offering an understanding of sedimentary history of the sea floor. An understanding of post-depositional alteration of strata, due to physical (e.g., resuspension) and biological (e.g., bioturbation) processes, is of particular interest in prodelta environments. Prodelta environments provide a source of sediment for transport, a high deposition rate, and a record of terrestrial environmental signals that attenuate as they move from the source. To create predictive models of sedimentation an understanding of how both deposition processes, and post-depositional (biological and physical) processes operate is required.

X-radiography of sediment cores is a fast, non-destructive technique for visualizing sediment properties and inhomogeneities. Features such as sediment contrast boundaries, gradients, interfaces, and anisotropy of sediment components which are created during deposition, or by subsequent benthic faunal activity, are manifested as variations in bulk density. Such variations show as prominent features in an x-radiograph, and can reveal information overlooked using other methods of analysis (Holyer et al., 1996).

X-radiography has been used in medicine since 1895 and by paleontologists since the early 1900's. Hamblin (1962) was the first to use x-radiography as a descriptive tool in sedimentary geology, investigating the internal structures of sedimentary rock thin slices to delineate sedimentation units in apparently homogeneous sediments. Use of x-radiography as an aid in providing descriptive analyses of sediment samples has been widely adopted, and increasingly

sophisticated methods developed (e.g., Bouma, 1964; Howard, 1968; Axelsson, 1983; Butler, 1992; Briggs et al., 1996). There are many examples in the literature that have used x-radiography in time-series studies, both long-term and seasonal. For example, Edmondson (1991) x-rayed both wet and dry cores from Lake Washington annually between 1965 and 1984 to study seasonal diatomatous sediment burial; the x-radiographs were used in a semi-descriptive manner alongside SEM images. Feng et al. (1998) described seasonal variations in near-surface sediments in the Hudson River estuary from x-radiographs, using the x-radiographs in a descriptive sense to support interpretations made from quantitative radionuclide and trace metal data. Use of x-radiography in pilot studies is common in the literature, for example, Brush et al. (1982) used x-radiography to detect laminations and texture differences in sediment samples prior to pollen and ^{210}Pb dating to rule out extensive post deposition mixing, and Mulder et al. (2001) used x-radiographs as a guide to locate appropriate sub-sampling sites for turbidite sequence studies.

Although the use of x-radiography as an aid in observations of sedimentary structures (e.g., Grimm et al., 1996; Santschi et al., 1999) and bioturbation (e.g., Howard, 1968; Smith et al., 2000) is extensive, a major limitation involved with the use of non-digitized x-radiography is the non-to-semi-quantitative nature of past studies. There is a need for improved methods of objective, quantitative analysis of the uppermost portion of the sedimentary sequence, as initial deposition and subsequent reworking of depositional layers create heterogeneities which are preserved by burial (Kuehl et al., 1995; Briggs et al., 1998).

The scanning of film x-radiographs into digital form first appeared in the literature in Holyer et al. (1996), where limited quantitative methods of texture analysis were developed. Briggs et al. (1998) developed image analysis techniques to allow comparison of digitized x-radiograph texture analysis to small-scale

variations in electrical resistivity that showed correlative results. Quantitative measurements of millimeter-scale sediment texture were also made in both these papers; however, no objective, quantitative strata measurements on centimeter scales were made.

The objectives of this study were threefold. First, techniques were developed to analyze x-radiographs, with the hope that these methods would prove to be more quantitative than those used by researchers in the past. Second, the techniques developed herein were used to map the initial distribution and mass of the October 2000 flood deposit from the Po River. Third, the post-depositional alteration of the Po deposit, between December 2000 and April 2002, was studied to quantify consolidation and estimate subsequent deposition and erosion. As a result of all these activities a greater understanding of episodic sedimentation processes was gained.

STUDY AREA

The study area is located near the Po River delta, in the northwest Adriatic Sea (Figure 1). The Po River is the largest in Italy, with a total catchment area of 70,091 km^2, and a length of 691 km (Nelson, 1970). Over 30,000 km^2 of the basin can be considered mountainous, with the Italian and Swiss Alps forming the northern rim of the basin, the Maritime Alps forming the western rim, and the Apennine chain rimming the basin to the south. Average annual discharge of the Po between 1918 and 1960 was 1,500 m^3/s. Average annual sediment load is 1.5 x 10^7 T/yr (Milliman and Meade, 1983); however, up to 4 x 10^7 T/month (implies 15,432 kg/s, or 3 g/L for 1 month of 5000 m^3/s discharge) sediment load was recorded during November flooding (Nelson, 1970). Annual discharge is

characterized by two main peaks; a fall-winter peak associated with rain storms (monthly average 1,900 m^3/s discharge and 1,150 kg/s sediment flux), and a spring peak associated with snow melt (monthly average 2,000 m^3/s discharge and 1,300 kg/s sediment flux) (Nelson, 1970). Since river gauging began in 1918, six major floods on the Po River have been recorded with daily averaged discharge exceeding 8,500 m^3/s. The last major flood prior to October 2000 was in November 1994.

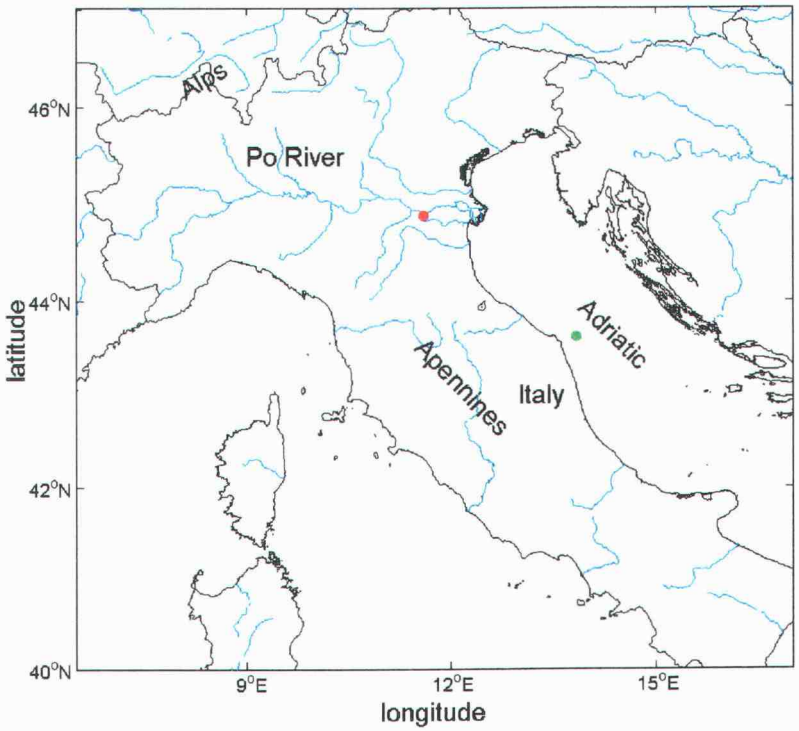

Figure 1. Map showing location of the Po River. Red dot is the location of Pontelagoscuro. Green dot is the location of the Ancona wave buoy.

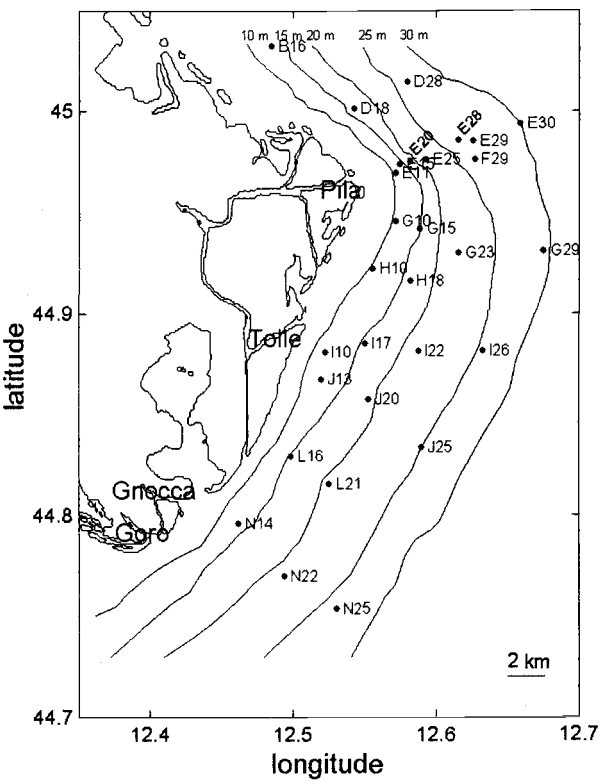

Figure 2. Map showing location of the December 2000 coring stations on the Po River prodelta and the position of the major distributaries.

The lower 50 km of the Po flows across a deltaic region, and discharges into the Adriatic via four main mouths; the Pila, Tolle, Gnocca, and Goro from north to south (Figure 2). The Pila is the main mouth, with an estimated 61 % of total water discharge and 74 % of sediment load. The Tolle, Gnocca, and Goro are estimated to discharge 7, 11, and 8 % of sediment load, respectively (Nelson, 1970). The Po delta, from Porto Levante in the north, to Sacca di Goro in the south, is 30-km wide, and has an area of 381 km^2. The prodelta extends approximately 9 km from the delta shoreline, which is scattered with numerous embayments, to approximately 30-m water depth, beyond which bottom slope is negligible (Figure 2). The modern delta has prograded over the last 400 years as a result of

anthropogenic alterations to the flow path of the Po. Venetian engineers, concerned that Po sediments would eventually infill the Venice Lagoon inlets, diverted the river southeast (Bondesan, 1990). This intervention was completed in 1604, and the delta has prograded seaward at an average rate of 60 m/yr between 1604 and 1992.

The sedimentology of the prodeltaic area in front of the Pila mouth consists of sands in < 10-m water depth, and a maximum thickness of Holocene muds of 10-12 m at a depth of 20-25 m (Boldrin et al., 1988). In recent years an increase in the number and duration of anoxic water column periods in late summer months has occurred (Justic, 1987). Eutrophication, due primarily to the Po River, has been documented to have increased in the last ten years along with a shift in dominant benthic foraminiferal species (Barmawidjaja et al., 1995). Macrobenthos densities on the prodelta have been found to peak in summer with predicable species assemblages and densities. However, in autumn and winter disturbances (e.g., oxygen depletion, large temperature drop, and flood deposition) can disrupt the community structure, minimizing species diversity until recolonization occurs the following summer (Ambrogi et al., 1990).

The northern Adriatic, a relatively shallow sea with few areas exceeding 50 m, was formed by the flooding of a fluvio-lacustrine plain during the Flandrian postglacial transgression that reached a maximum around 2,000-3,000 yr B.P., with the area around the Po River study site being flooded around 6,000 yr B.P. (Boldrin et al., 1988; Colantoni et al., 1979). The Adriatic Sea is considered a low energy environment; Ancona wave buoy data ($43^0$37'00''N, $13^0$51'00''E, Figure 1) shows a mean wave height of 0.7 m ± 0.55 m (s.d, n = 9,518), an average of 21 d/yr with >2-m height, and a maximum wave height of 4.2 m over a 3.3-year period between January 1999, and April 2002 (envirtech.org). Average tidal range in the region is around 60 cm (Nelson, 1970). The predominant currents in the northern Adriatic

flow anticlockwise around the basin perimeter. Thus, currents in the study area carry suspended sediments from the Po in a southerly direction down the Italian coast in a narrow coastal region (Kourafalou, 1999), such that the deposition of mud in the north-western Adriatic is limited to a belt along the Italian coast (Van Straaten, 1965; Catteneo et al., in review).

In October 2000 a major flood occurred on the Po River with a maximum daily averaged discharge on October 20 of 9,650 m^3/s, a discharge exceeded only twice since 1918. Maximum rainfall of more than 700 mm was recorded in western regions of the catchment, and over 40,000 people were evacuated from their homes. The flood was characterized by five main peaks stretched over 53 days as a result of discharge time lag from the large drainage basin (Figure 3). The occurrence of this flood prompted this event-response study.

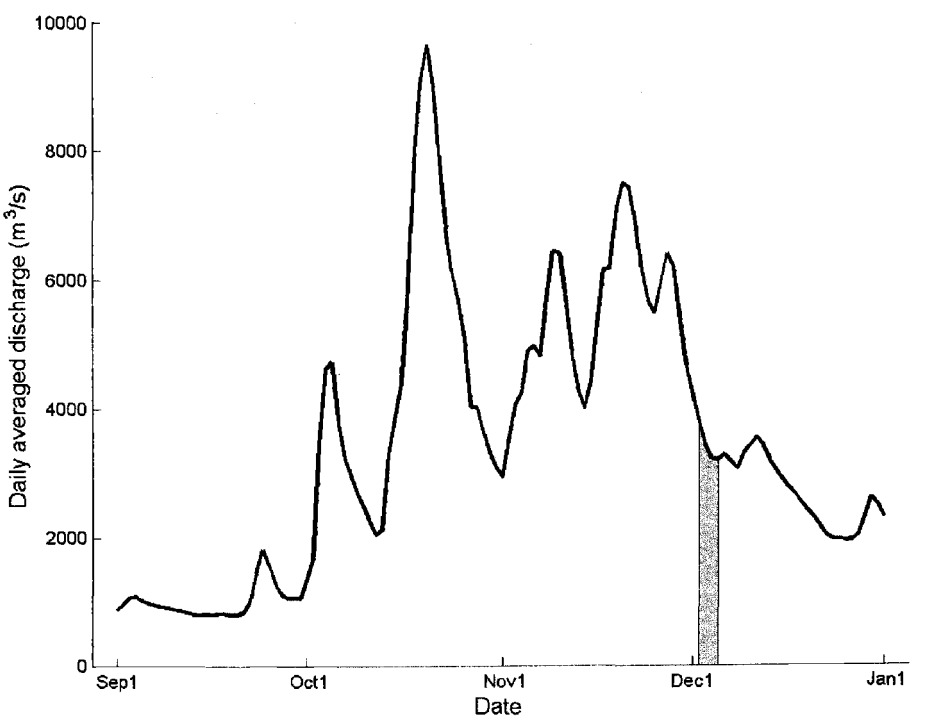

Figure 3. Averaged daily discharge of the Po River during the October 2000 flood measured at Pontelagoscuro (see Figure 1). Shaded region indicates dates of the December 2000 coring cruise. Source: Regione Emilia –Romagna. (2001)

METHODS

FIELD SAMPLING

Data

An initial event response investigation of the October 2000 flood was carried out in December 2000 (Figure 3). Sediment samples were collected (onboard the M/V Sarom VIII, a 26-m gas platform tender) using an Ocean Instruments box corer (20 x 30-cm cross-sectional area with a maximum 60-cm depth). From each box core, two samples were taken for x-radiography. The pair of samples from each core were taken orthogonal to each other near the edges of the box core to allow for additional sub-sampling. Additional cores were collected during three subsequent box-coring cruises (Table 1). During the April 2002 cruise, kasten cores were taken in addition to box cores at 12 sites within the study area. The primary purpose of these deeper cores (up to 2 m deep) was to analyze natural radionuclide content (e.g., ^{210}Pb); however, x-radiographs were taken down the entire core length of each kasten core and used in this study.

Table 1. Box core sampling dates and data totals, 'December 2000 repeats' represents the number of December 2000 stations cored on a given cruise

Cruise	Coring dates	Total stations cored	December 2000 repeats	# replicate stations (# replicates)
Dec 00	2-5	33		
Jun 01	4-6	27	23	2 (2) (2)
Oct 01	11-15	74	22	2 (3) (4)
Apr 02	20-22	31	21	1 (2)

Stations

Sampling stations were named with a letter and number; the letter denotes the transect line, and the number denotes the station water depth in meters (Figure 2). Beginning north of the Pila, the transect lines run approximately normal to the coast and were spaced roughly 3 km apart, with the 'E line' directly off the Pila mouth, the 'I line' just south of the Tolle mouth, and the 'N line' off the Gnocca mouth. Stations were spaced at approximately 5-m depth increments along each line between 10-m and 30-m water depth; the seven stations on the E line covered a total distance of 7.4 km between E11 and E30.

Collection

The aim of the field sampling cruises subsequent to December 2000 was to reoccupy previously cored sites off the Po River. The average differential-GPS co-ordinates for each station from prior coring cruises were used as target co-ordinates. Typically one box core was taken at each station and processed immediately on the ship's fantail. Supernatant water was siphoned off the top of each core before removal from the frame and transfer to the processing area.

Samples were taken from the box core using rectangular polycarbonate x-ray trays (Figure 4A). Two trays with the face plates removed were inserted in each box core orthogonal to each other (e.g., Figure 4B). The trays were first dipped in water to minimize friction with the sediment. The faceplate was then inserted, causing the sediment inside the x-ray tray to compress a small amount. Measurements of height difference between the sediment surface in the box core and inside the tray indicated this compression was approximately 5 %. The box core face plate was then removed and the base caps inserted under each tray. The

trays were lifted out, surficial mud was cleaned off, and the caps were taped on. The x-radiograph was shot onboard, typically within 30 minutes of core collection.

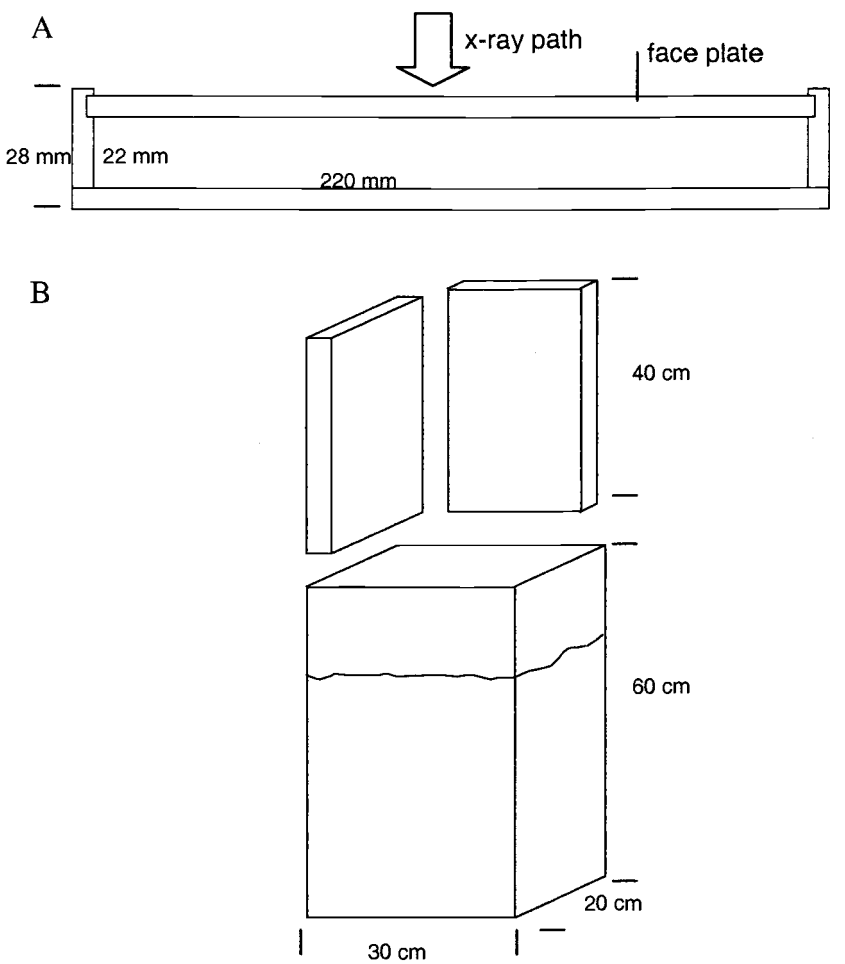

Figure 4. (A) X-ray sample tray plan view, (B) box core showing sample trays in orthogonal sampling arrangement

X-RADIOGRAPHY

X-radiography records a signal level proportional to the transmittance of x-rays as they irradiate a sample. X-ray attenuation is predominantly dependant on the volumetric electron density of the attenuating substance, and slightly dependant on the atomic number of the substance and the wavelength of radiation (Holyer et al.; 1996, and Axelsson, 1994). Volumetric electron density is related to gravimetric density, thus x-radiograph light transparency is almost a linear function of gravimetric density (Holyer et al., 1996). The transmitted x-ray fraction (I/I_0) is given by

$$I / I_o = e^{-\mu x},$$

where x is the material thickness, and μ is the total linear x-ray attenuation coefficient (Karellas, 1997). Orsi et al. (1994) demonstrated this direct relationship by comparing the response of their x-ray scanner and the wet bulk density of laboratory samples to find a linear relationship ($r^2 > 0.99$). Briggs et al. (1998) found a linear relationship between x-ray transparency and porosity, the predominant contributor to sediment bulk density fluctuations, i.e.,

$$\rho_b = (1-\varphi)\rho_s + \rho_w\varphi,$$

where φ is porosity and ρ_b, ρ_s, and ρ_w are the bulk, sediment and water density respectively. Regions in a sediment sample with low bulk density are more x-ray transparent and hence when x-rayed record a lower brightness level. Thus the spatial distribution of brightness in an x-radiograph is considered to reflect the spatial structure of sediment density (Holyer et al., 1996).

The x-radiographs in this study were taken using a Lorad LPX-160 industrial x-ray generator and a dPix FlashScan 30 amorphous-silicon imager. The transportable x-radiography system is housed in a 16-mm thick lead cabinet (Figure 5), from which the system can be removed for ship use. Sample trays are placed 168 cm from the x-ray source against the imager. A brightness calibration strip of known density was placed along side each x-ray slab. Samples were typically exposed at 70 kV, 5 mA for 6.4 s. The imager converts x-ray energy to visible light energy, the light energy is in turn converted to photo charge and accumulated by each pixel to produce a 12 bit (4096 grayscale) image with a 127-μm pixel spot size that is 29-cm wide by 40-cm high.

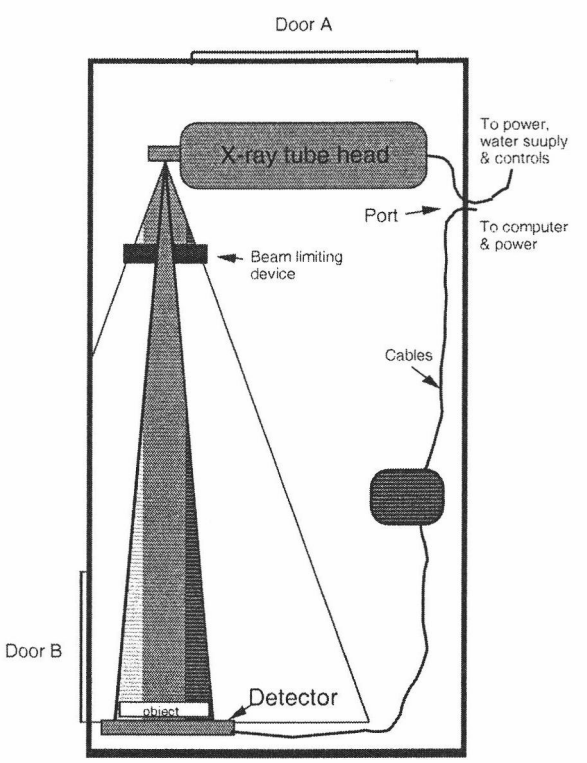

Figure 5. Plan view of digital x-radiography system. Samples are placed against the detector (imager) through door B. The tube head (x-ray source) is removable through door A.

Unfortunately, most of the images had an artifact that resulted in the right half of the image being brighter. This brightness offset affected the same area in each image; however, the magnitude of the offset differed between images, and often within images. The offset was greater towards the top of the affected region, and greater in pixels with lower brightness. To reduce the offset, the image was cropped to show only the sediment, and the brightness of each column of pixels averaged to find the mean intensity of the offset. A corrective image was produced with zeros in the columns right of the offset, and the corrective value equal to the average intensity of the offset in the remainder of the columns. The corrective image was then added to the cropped image. This procedure removed the majority of the offset leaving only the difference in offset within in the range of sediment brightness – typically a minimal difference.

DETERMINING THE FLOOD DEPOSIT THICKNESS

Three different properties of newly deposited sediment were investigated to create objective methods of deposit thickness measurement. The bulk density, basal edge, and texture change at the deposit base were each investigated as a means of locating the deposit basal contact.

Bulk Density Method

Newly deposited flood layers have been observed to have high porosity and hence low bulk density relative to the underlying sediment (Wheatcroft et al., 1996; Wheatcroft and Borgeld, 2000). This contrast exists because newly deposited sediment requires time to consolidate, and flood sediment is often finer grained

than sediment deposited during non-flood conditions. The lower bulk density of the flood deposit is recognized in the x-radiograph as a change in brightness. A sharp increase in bulk density down-core, seen as an increase in image brightness, is assumed to mark the base of the flood deposit (Figure 6A). Ideally a brightness histogram results in a bimodal distribution and the trough between the two peaks could be used to objectively segment the image (Figure 6D). The resultant binary image could be used to measure deposit thickness (Figure 6B). To provide small-scale spatial variability information, thickness is measured at five equally spaced positions in each x-radiograph.

Edge Contact Method

If the pre-flood seafloor were relatively flat, then one would expect a recently deposited flood layer to have an abrupt edge with the underlying sediment (i.e., a contact). The contact would be a continuous horizontal edge, caused by differences in sediment properties such as porosity, grain size and centimeter-scale texture between the two layers. This contact would presumably be sharp initially, and would become blurred over time as contrasting properties were mixed by biological (e.g., Hanor and Marshall, 1971), or physical (e.g., Nittrouer and Sternberg, 1981) processes.

A horizontal edge detection algorithm was created for finding the basal contact of the flood deposit. The edge detection algorithm produced an 'edge map' the size of the original image with pixels above a certain brightness corresponding to horizontal edges in the x-radiograph (Figure 6C). The first step in producing the edge map was to remove *vertical* edges, caused for example by burrows or shell debris, by producing an image where each pixel was set equal to the average value of the 10 pixels to the immediate right and left of the corresponding pixel in the

original image. This step averaged out vertical edges, but maintained horizontal edges. Next an investigation of a subset of images collected on the December 2000 cruise found the average contact to be 2-mm (15 pixels) thick. Thus the edge map algorithm looked for a horizontal edge by calculating the maximum range between pixels 20 rows apart. This second step created the edge map by assigning each pixel the brightness-range value of the ten pixels above and the ten pixels below the corresponding pixel in the image produced in step one.

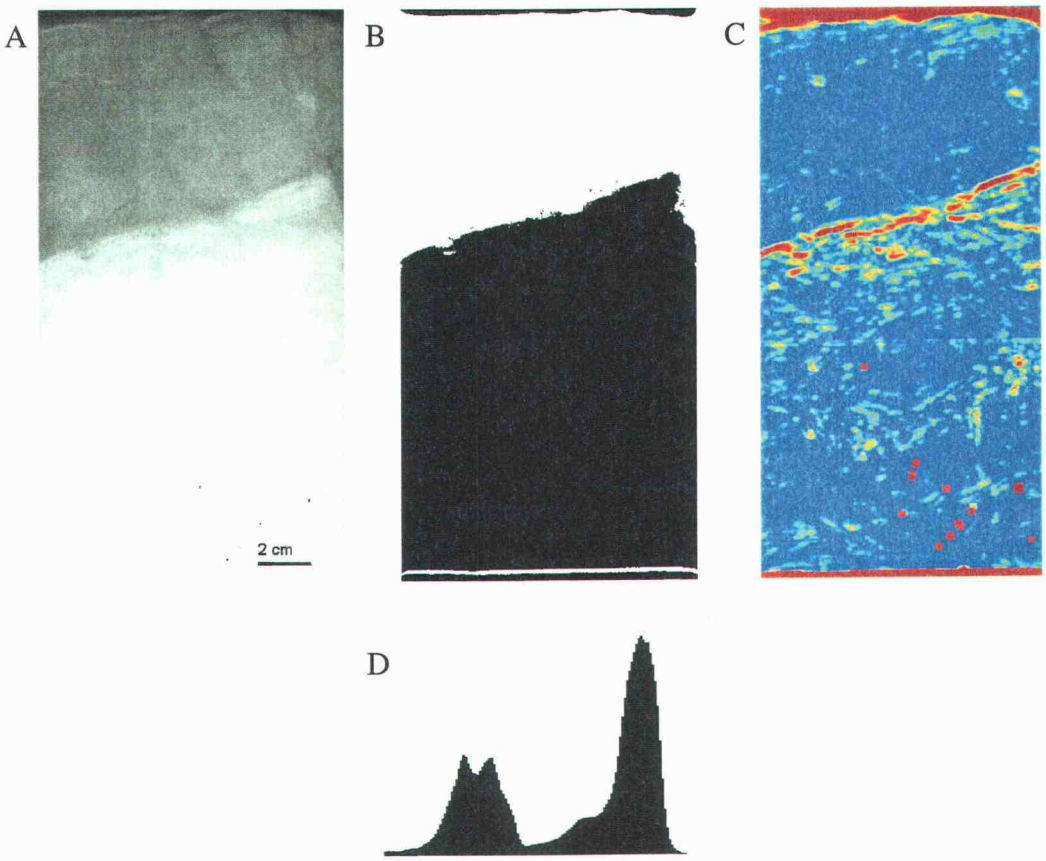

Figure 6. An example image from station E28 showing images used in determining flood deposit thickness, (A) original image (B) bulk density threshold (C) edge map (D) brightness histogram (x-axis runs from dark pixels (left) to light pixels (right)).

A contact was considered to be any line of pixels, with a value exceeding a threshold, which extended horizontally for more than two thirds of the edge map. The threshold was set at 75 % of the total range of pixel values in the edge map, which corresponded to approximately 2 % of the pixels, and was typically a pixel range of 140 grayscales. The threshold for determining a contact was chosen through trial by segregating deposit basal contacts from sub-deposit horizontal edges – which are typically less than two thirds of the image width and less bright than a deposit basal contact. The distance from the top of the sediment to the deepest contact was measured at five equally spaced points in each image to provide centimeter scale variability information. The distance to the deepest contact in an image was measured, as many images contained multiple beds (see discussion below).

Texture Method

Benthic infaunal activity mixes the sediment within a layer predominantly near the sediment-water interface, thereby homogenizing sediment fabric (e.g., Hanor and Marshall, 1971). Deposition of new material at the sediment-water interface shifts all subjacent material downward relatively. Therefore, in cases where a new flood deposit covers the previous surficial, bioturbated sediment, the old sediment-water interface and bioturbating infauna are buried. The new deposit requires some time to become colonized and bioturbated by benthic fauna. Until recolonization occurs, the newly deposited sediment retains its depositional structure of horizontal layers of differing bulk density. Hence the structural appearance of the sediment in the two layers should differ, providing a simple but quantitative caliper for estimating event bed thickness (cf. Wetzel and Aigner, 1986).

Texture analysis was used to locate the buried sediment-water interface. Texture is defined by Briggs (1998) as 'the local spatial distribution of tonal values within an image'. Measurements of texture involved use of various combinations of neighbor operations such as range, variance, Sobel, Hurst and Haralick operators as defined in Russ (1996, p. 361), as well as the binary run length method described by Holyer et al. (1996). Each of these methods was found to be applicable to segmenting a greater change in texture than was present across the basal contact in the x-radiographs. Texture maps of each image were produced using a 20 x 20-pixel (2.5 x 2.5-mm) floating mask to calculate the standard deviation of pixel brightness surrounding each pixel in the original image. The mask highlighted high brightness variation on several-millimeter scale, a scale found appropriate for viewing sediment texture created through reworking in the x-radiographs after trial of differing mask sizes. The texture maps produced were useful as an interpretive tool (see below), but objective measurements of deposit thickness were not made from the texture maps as the maps contained too much noise to enable thresholding.

Eel River Data Comparison

The methods developed herein for determining the flood deposit thickness were tested against a set of x-radiographs of a previously studied flood deposit off the Eel River, northern California. Wheatcroft and Borgeld (2000) showed that Eel River flooding during January 1995 produced a deposit on the continental shelf north of the Eel River extending ~ 30 km along-shelf and 8 km across-shelf. Subsequent floods in March 1995 and January 1997 produced distinct deposits with similar distribution to the January 1995 flood. Box cores of the deposit were collected on nine cruises between February 1995 and July 1998 at 40 to 70 stations per cruise. X-radiographs were shot onto film and analyzed visually. The deposit

thickness data from the x-radiographs, backed with independent ^{7}Be geochronology (Sommerfield et al., 1999), grain size, and micro-scale porosity profiles, were published by Wheatcroft and Borgeld (2000).

The x-radiographs from the Wheatcroft and Borgeld (2000) analysis were used as a methods check for the techniques developed for analysis of the Po River x-radiographs. The images from both February 1995 and January 1997 along the 70-m isobath were scanned at 200 dpi (127-μm pixel size) using a UMAX PowerLook 1100 scanner, and both the bulk density method and edge contact method were used to objectively determine the deposit thickness for comparison with the thickness values reported by Wheatcroft and Borgeld (2000).

FLOOD DEPOSIT EVOLUTION

Total Thickness Change

To evaluate temporal change in flood deposit thickness, images taken during the June 2001, October 2001 and April 2002 cruises were compared to the original December 2000 x-radiographs (Table 1). Stations were selected for analysis according to three criteria. First, the December 2000 flood deposit thickness had to exceed 1 cm. This criterion eliminated sites peripheral to the main deposit, where measurements of the deposit thickness after several months would have been difficult to make objectively, due to the high mixing rates of the upper portion of the bed. The second criterion was that images from sites cored in December 2000 were available from at least two of the following three cruises. Third, the deposit base, as determined from the deepest contact on the edge detection map, had to be visually detectable in the December 2000 image. This third criterion allowed increased accuracy in the estimate of temporal deposit

thickness change from the remaining sites. The selection process described above removed 17 of the 29 December 2000 stations from further analysis. Removal criteria are shown spatially in Figure 7.

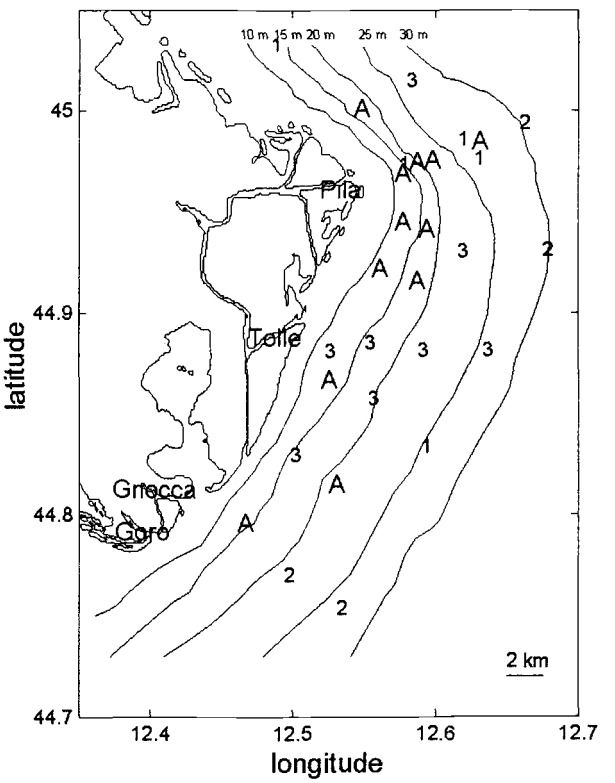

Figure 7. Map showing selected stations for total thickness change analysis (A) and stations removed from analysis with the removal criterion. 1 = not cored on each cruise; 2 = Dec 00 deposit < 1 cm; 3 = Dec 00 contact not clear.

Typically there were a total of eight images for each of the 12 stations analyzed – the orthogonal pair from the core from each of four cruises. A vertical reference horizon was determined from viewing each of the eight images. The reference horizon was chosen as a contact that was distinct, hence readily recognizable, and present in the maximum number of images. If both the deposit base, and internal contacts were present, then the basal contact was used. The contact was then marked on each image, and the corresponding edge detection map

was used to make a measurement of the distance between the contact and the sediment-water interface. Stations where the reference horizon was visible in only one image were still used, and if more than two images were available from a station on any one cruise then all the images were used and the resulting thickness estimate averaged.

Consolidation

In theory, conversion from pixel brightness values to bulk density can be calculated based on calibration targets of known density included in each image (Figure 8). The bulk density of certain deposit beds, that are distinct and present in the time series of images, could then be measured over time to calculate a consolidation rate.

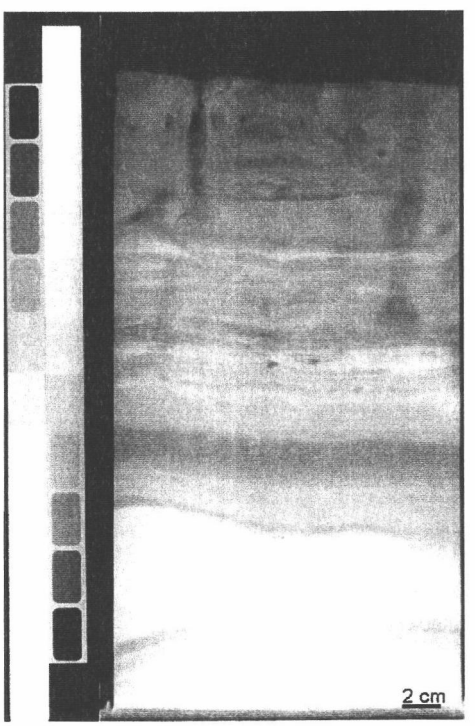

Figure 8. X-radiograph from station E16 in October 2001 showing density calibration target.

Three calibration targets were used over the course of the four cruises containing known density bins (Figure 9). The brightness response of the three targets shot at 70 kV showed that the glass (GL) and aluminum (AL) targets have similar brightness response for a given density (Figure 10). The ceramic target (CE) was omitted from use after December 2000 as the small bins allowed edge refraction effects over the entire bin. The bins in CE sat up to 22 mm from the image (target thickness was 28 mm, the lowest density bin was created from a 6-mm long cylinder of ceramic). The ceramic cylinder used to create the bin was only 3.5 mm in diameter and hence beam refraction greater than 1.2 degrees affects every pixel in the bin. AL and GL had much larger bins (>324 mm^2 verses 10 mm^2 for CE).

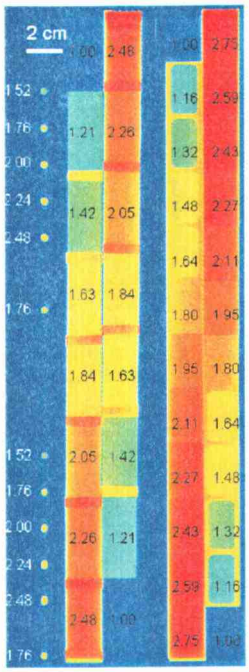

Figure 9. Pseudo-color x-radiograph showing the three targets used (CE, GL and AL, left to right). Values indicate independently calculated densities in g/cm^3 of each bin.

The relationship between density and brightness for AL and GL is defined by,

$$\rho = (2.51\times10^{-7}b^2) - (4.98\times10^{-4}b) + 1.25,$$

where ρ is density and b is brightness ($r^2 = 0.98$). This equation allows conversion of brightness measured within a deposit bed to bulk density, independent of the target type included in the image.

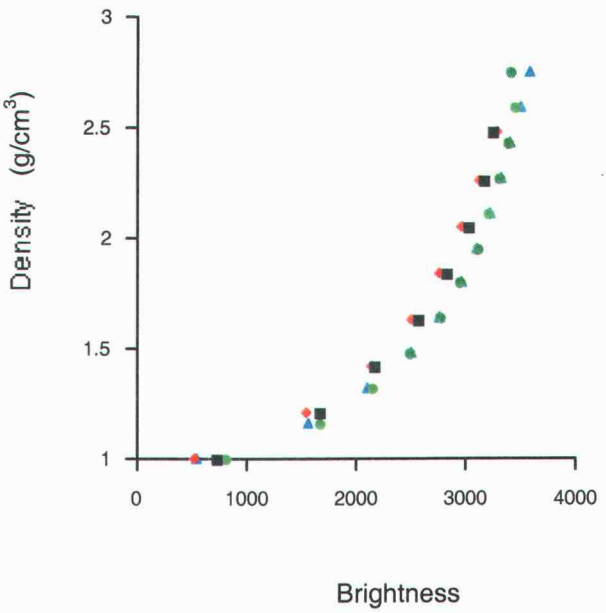

Figure 10. Brightness response of known density target bins for targets GL and AL. Black square and red diamond are the left and right strip respectively of target GL, green circle and blue triangle are left and right strip respectively of target AL.

Before applying this technique, x-ray beam pattern was removed from each image. The x-ray beam directed at a sample being imaged is concentrated on the central lower portion of the image, creating lower apparent brightness in this region as more x-rays pass through the sample. The beam pattern was imaged using a piece of PVC of uniform thickness which allowed the pattern to be mapped at a similar density to the sediment samples, on a surface with homogenous density.

The PVC image showing the beam pattern was used to make a beam correction map. The correction map was created by subtracting the mean PVC image pixel brightness from each pixel in the PVC image (Figure 11). The correction map, with negative values in the central lower portion, increasing towards the upper corners, was then subtracted from each original sample image used in the following analysis.

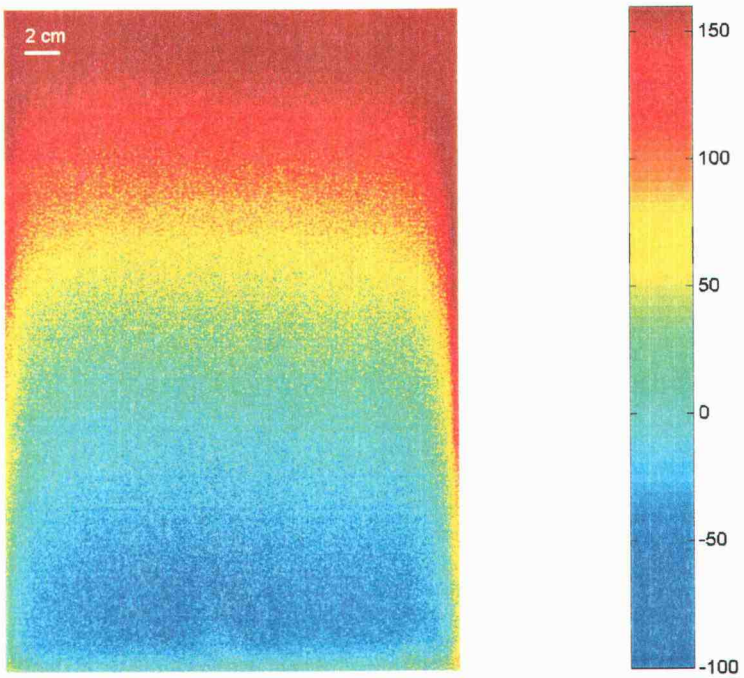

Figure 11. Beam correction map showing the x-ray beam pattern. The color bar represents the brightness difference of each pixel from the mean image brightness.

To estimate increase in sediment bulk density from an increase in image brightness over time at sites evaluated for total thickness change, all the images from a single site were viewed and deposit beds were selected from which to assess the increase in brightness. The mean pixel brightness in each layer was calculated.

A second method used to estimate consolidation within the deposit was to measure the change in thickness of a bed within the deposit. To make these measurements a distinct bed, >1-cm thick, with a distinct horizontal contact both above and below was marked over the time series of images at a particular site. Edge detection maps for the time series of images were then used to measure the distance between the upper and lower contact of the bed.

Small-Scale Spatial Variability

To determine the significance of deposit thickness measurements over time, an estimate of variability over small spatial scales is needed. Repeat cores were taken at several sites during the later three cruises (Table 1) to investigate the spatial variability in deposit thickness on the same scale as occurs when stations are re-cored on subsequent cruises. For stations cored more than once over the four cruises, the station mean latitude and longitude were calculated and residuals of each core site from the station mean were calculated. The mean residual was 31 m ± 2.3 m (s.e., n = 114). The significance of deposit thickness variability on this tens-of-meters scale allows understanding of the significance of temporal thickness changes observed at a station.

The repeat cores from a single station were marked at a reference horizon, and the depth to the horizon measured from the edge detection map, as with determining temporal change in deposit thickness at a site. However, a reference horizon could not be found in either set of June images. The repeat cores from the other three sites were measured and analyzed using a nested analysis of variance (NANOVA), a standard statistical procedure (Sokal and Rohlf, 1981, p. 274) to deduce whether the variance in the deposit thickness measurements arose predominantly from thickness variation within an image (centimeter scale),

between the orthogonal pair of images within one core (tens-of-centimeters scale), or between repeat cores within a station (tens-of-meters scale).

RESULTS

DETERMINING THE DEPOSIT THICKNESS

Bulk Density Method

The flood deposit thickness, calculated using the bulk density method at each station cored in December 2000, is greatest proximal to the river mouths (Figure 12). Maximum deposit thickness using the bulk density technique was 23 cm at station J13; however, the stations directly adjacent to the Pila mouth were not measured as they did not have a bimodal brightness distribution. Detection of the deposit is restricted to stations in less than 30-m water depth.

Seventeen out of 29 stations had a bimodal brightness distribution in at least one image, and the thickness of the deposit at those stations is shown (Figure 12). The remaining 12 stations that lacked bimodal brightness distribution were assigned a '1' in Figure 12 if there was minimal brightness change in the image, and a '2' if apparent bulk density change existed in the image but was not bimodal (e.g., multiple bedding, x-ray opaque sediment in deposit). This method produced a result in 23 out of 56 total images. The deposit thickness at the six stations where thickness could be estimated from both images had a fractional uncertainty of $\pm$ 11 % ($\sigma / \langle x \rangle * 100$).

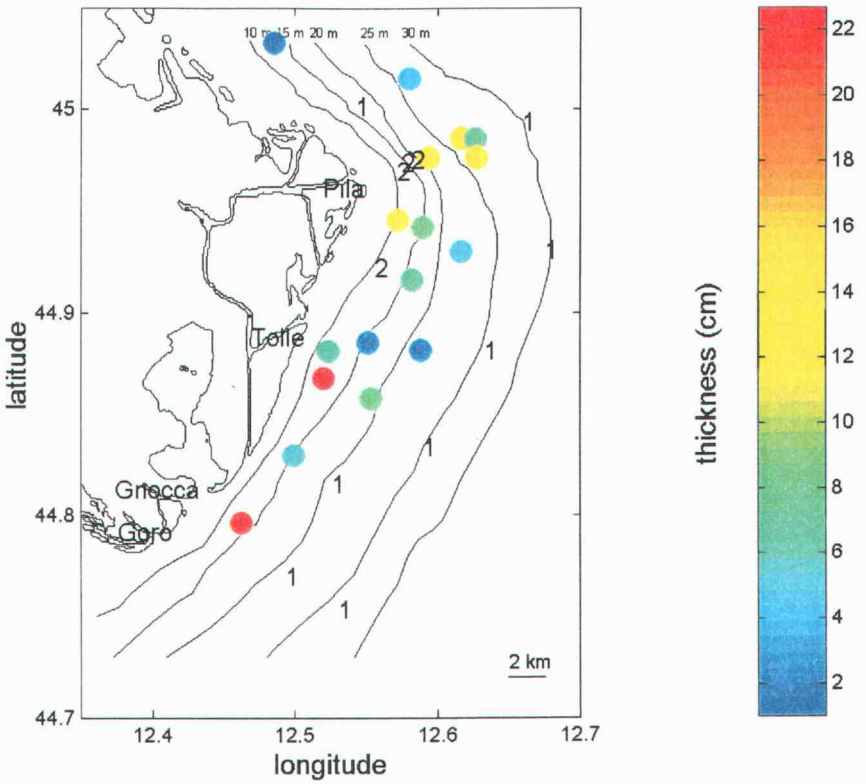

Figure 12. December 2000 deposit thickness estimated using bulk density method. Stations with non-bimodal brightness are marked as no density change (1), or density banding (2)

Edge Contact Method

Flood deposit thickness calculated using the edge contact method yields a similar pattern to the brightness technique (Figure 13). The deposit is thickest proximal to the river mouths, and is concentrated around the Pila mouth. Maximum flood deposit thickness was 26 cm at station E11; however, this estimate is a minimum due to the multiple contacts described below. The deposit has a sharp thickness gradient; confined to areas < 30-m water depth, the thickness

ranges from the 26 cm at E11 to the deposit edge between E29 and E30 in less than 7 km.

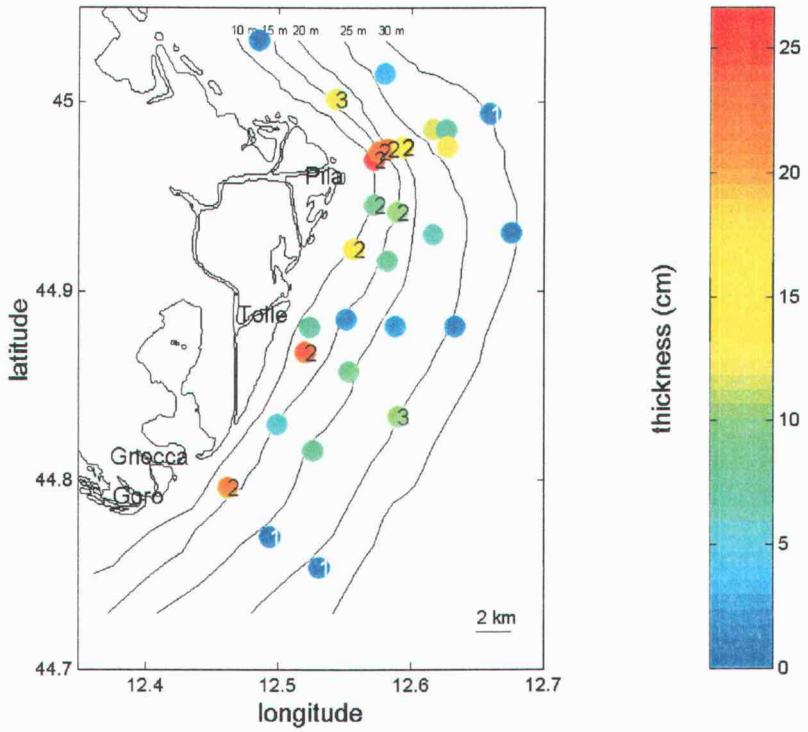

Figure 13. December 2000 deposit thickness using edge contact method. Stations with no contact present marked (1), stations with multiple contacts marked (2), station where thickness was determined incorrect marked (3) (see text)

A '1' was assigned to stations where no contact was present in the edge map; this was interpreted as no flood deposit present, and was typically found in stations in more than 25-m water depth (e.g., E30, N25). A '2' was assigned to stations where multiple contacts were present, and the thickness shown is that of the deepest contact to pass the criteria described in the methods section (Figure 13). Thickness values with a '2' assigned were interpreted as a minimum flood deposit depth, as it is possible additional contacts would be observed deeper in the sediment below the depth reached by the core. Such stations were found proximal to the river mouths (e.g., E11, G10, H10, N14), and included all four stations

marked '2' in Figure 12 (E11, E15, E20, H10). Station J25 and D18 were assigned a '3' as they were later interpreted to be a false result, but the thickness reported at these two stations in Figure 13 was the output given using the edge contact method. The false results are discussed in the texture analysis section.

Method comparison

A comparison between deposit thickness measured by the bulk density and edge contact methods, for the 23 images providing a result from the bulk density method, shows consistency between the two methods. There is strong correlation with a correlation coefficient of 0.99 (n = 23) (Figure 14).

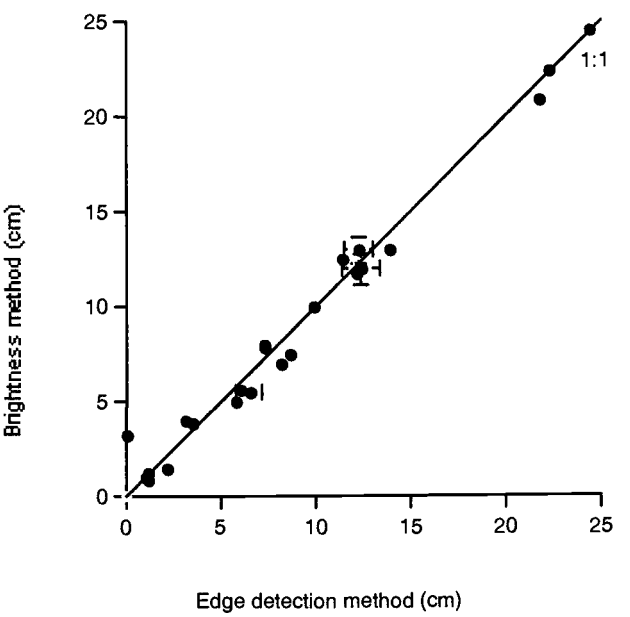

Figure 14. Deposit thickness method comparison for December 2000 images (correlation coefficient 0.99). Error bars indicate s.e. of 5 measurements per image, note that many error bars are smaller than the plot symbol.

Texture Analysis

The texture maps were used as interpretive tool to check results obtained from the bulk density and edge detection methods. For example, the edge contact algorithm detected a contact at 10-cm depth for station J25. This result is considerably thicker than surrounding stations and expected values for a station at 25-m water depth. The texture map at this site showed no difference in sediments directly above and below the contact (Figure 15), suggesting the contact was not the deposit base. Thus the detected contact was presumed to be below the deposit basal contact, and the thickness at J25 was recorded as a false result.

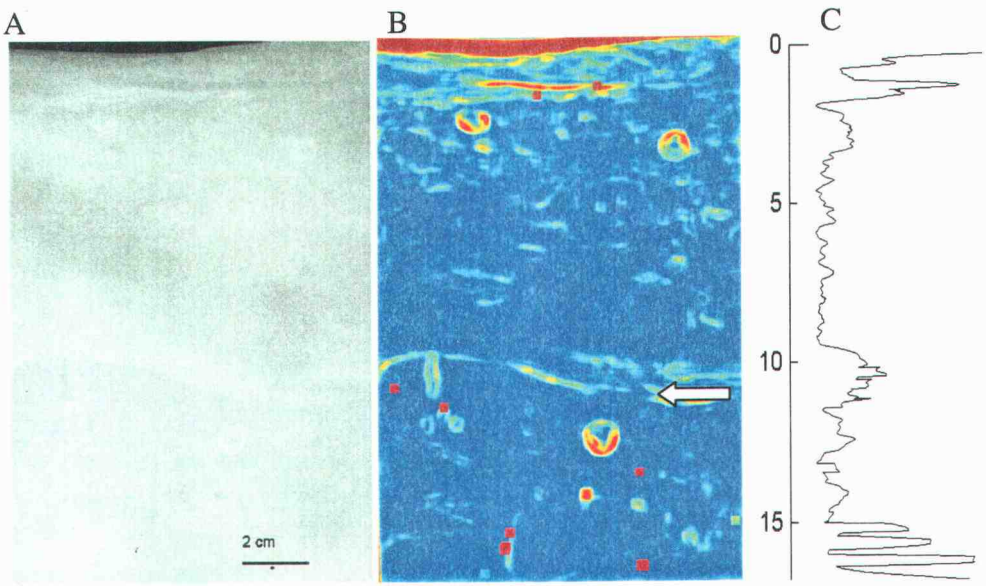

Figure 15. (A) An example image from J25 showing use of the texture map (B) to determine the false deposit depth at 10 cm (marked with arrow), (C) row average plot of the texture map with scale in cm. Note that the large signals > 15-cm depth are due to an imager artifact.

Texture maps were also used to interpret results from stations where both images had multiple contacts. The images from these stations were viewed alongside the corresponding texture map, and an observation of whether texture

change occurred below the deepest contact was made. Of the nine stations that had multiple contacts (Figure 13), six were observed to have increased texture variability below the deepest contact, suggesting the correct deposit basal contact was found (e.g, J13, Figure 16). The remaining 4 sites, E11, E15, E20, and E25 were presumed to have deposit thicknesses greater than the image depth. Kasten core x-radiographs were available from E11 and E20, and were used to measure deposit thickness using the edge map and texture map. Deposit thickness at E11 was inconclusive, as none of the images down to 150-cm depth showed a contact with texture change directly below, possibly as a result of continuous deposition at this site. However, E20 showed texture change below a contact at 38-cm depth which was interpreted to be the base of the flood deposit.

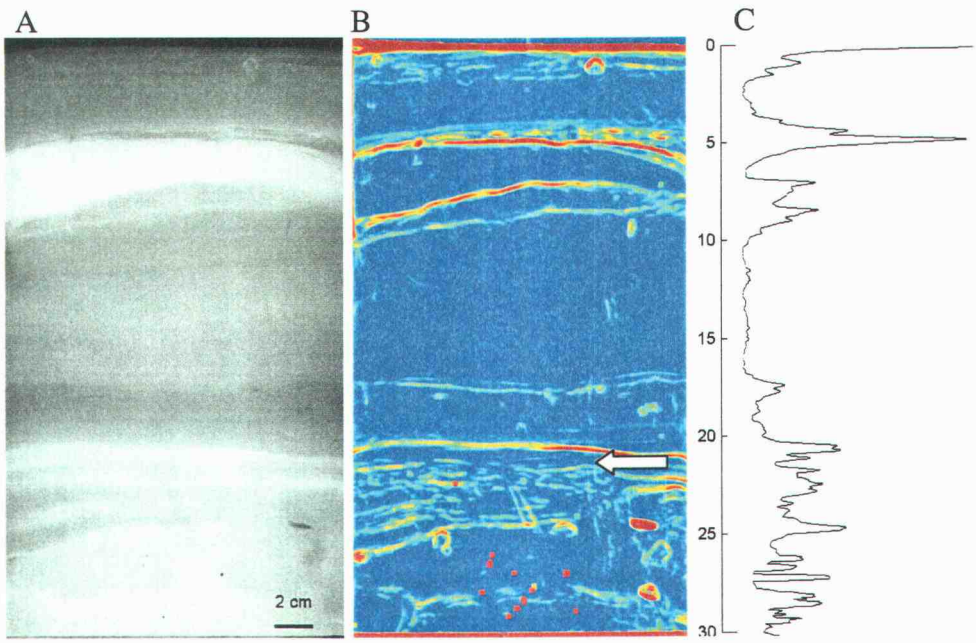

Figure 16. (A) an example image from J13 showing use of the texture map (B) to determine correct deposit depth at base of bedding (marked with arrow), (C) row average plot of the texture map with scale in cm.

Eel River Comparison

Comparison of the objective methods developed herein, to the multiple methods used by Wheatcroft and Borgeld (2000), showed high correlation in the February 1995 images (Figure 17A-C). Twelve sites along the 70-m isobath on the Eel Margin were investigated, and the two objective methods gave deposit thickness values with a correlation coefficient of 0.97. The mean of these two values was then compared to the results obtained by Wheatcroft and Borgeld (2000), and a correlation coefficient of 0.96 was found. With the removal of one site the correlation coefficient rose to 0.99.

Deposit thickness values obtained from January 1997 image from 15 sites along the 70-m isobath using the two objective methods were also highly correlated with a correlation coefficient of 0.98 (Figure 17E). These values were then compared to the Wheatcroft and Borgeld figures. Three of the fifteen sites had large differences in the comparison that are explained in the discussion. With these three sites removed, the correlation coefficient was 0.95, but with the three sites included the correlation coefficient dropped to 0.29.

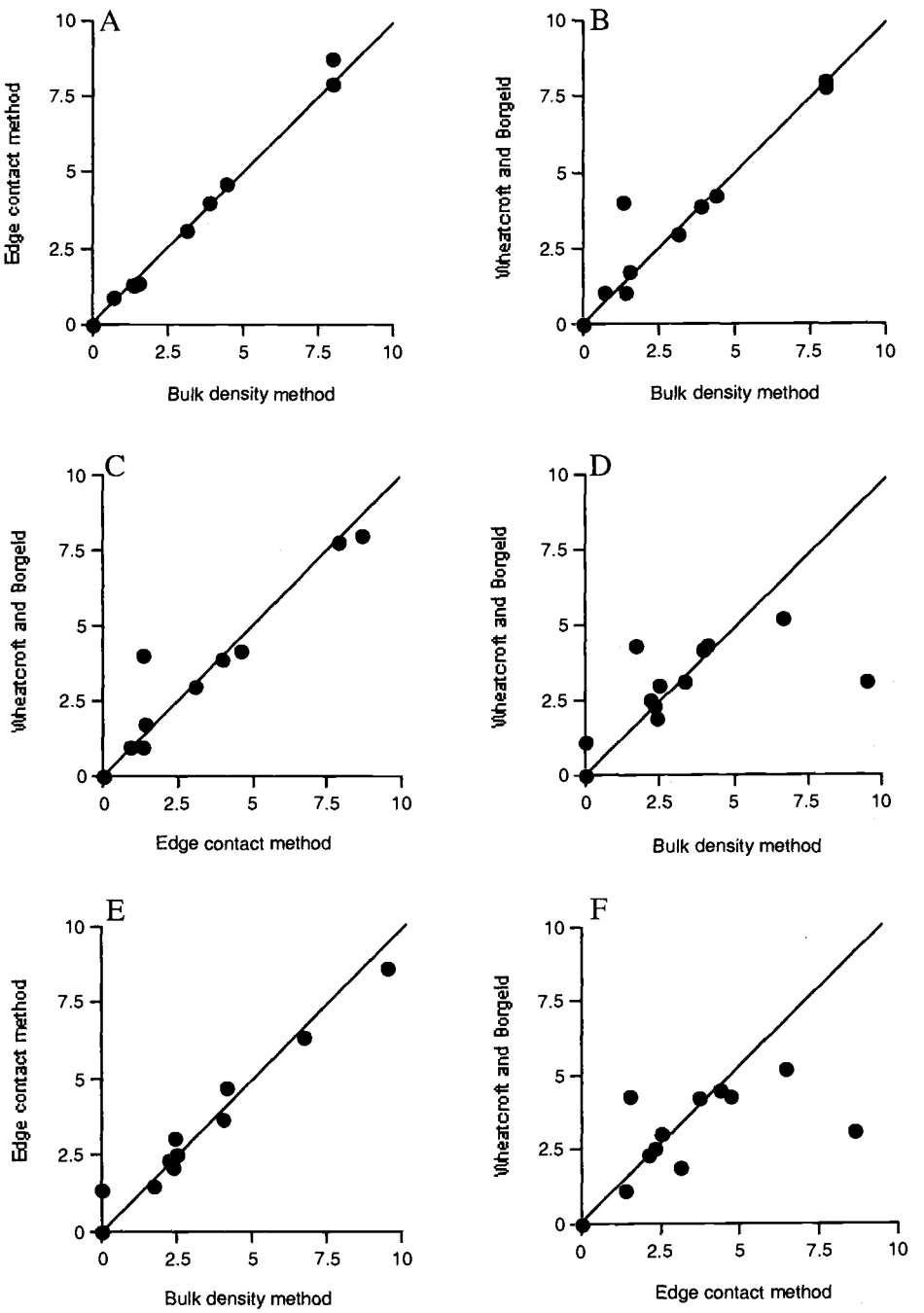

Figure 17. Eel River data comparison plotted with a 1:1 line, (A) 1995 deposit edge contact and bulk density, (B) 1995 bulk density and Wheatcroft and Borgeld 2000 (W&B), (C) 1995 deposit edge contact and W&B, (D) 1997 bulk density and W&B, (E) 1997 deposit edge contact and bulk density (F) 1997 deposit edge contact and W&B.

DEPOSIT EVOLUTION

Total thickness change

Measurements of total thickness change were possible at roughly a third of the December 2000 stations. Figure 18 shows the change in depth of the reference horizon between December 2000 and April 2002. At many stations there was continued deposition between December 2000 and June 2001, with a maximum at station E11. In contrast, stations E29 and N14 had net erosion after June 2001.

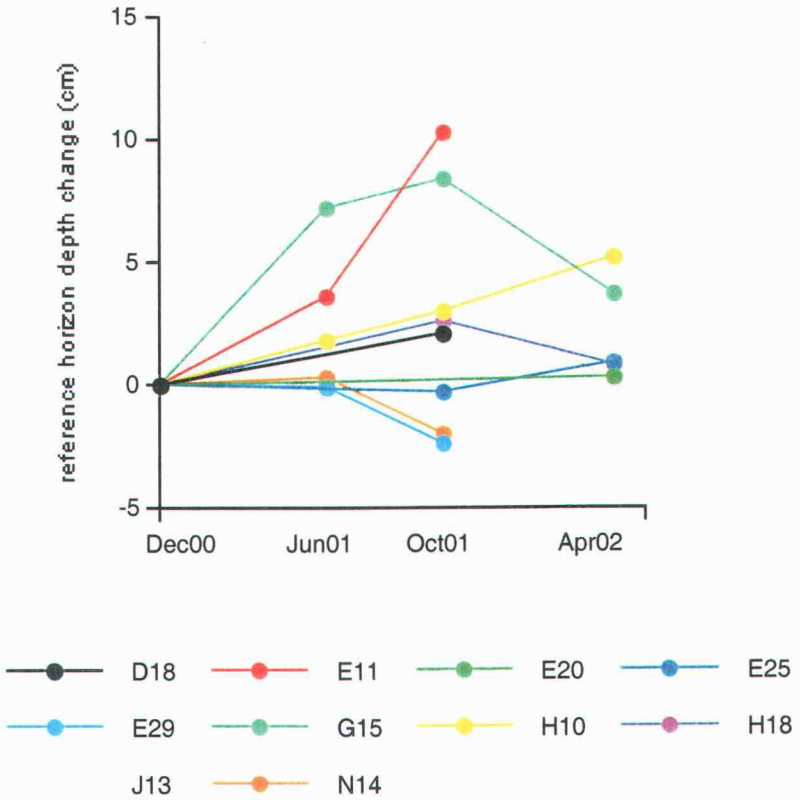

Figure 18. Total thickness change between December 2000 and April 2002. Note thickness is not necessarily the deposit thickness, as in some cases a silt layer was used to trace deposit thickness change.

Total thickness change between December 2000 and April 2002 (those marked 4 cruises in Figure 19) or October 2001 (those marked 3 cruises in Figure 19) for the 10 stations measured is greatest proximal to the Pila. The values range from 12 cm/yr at E11, to -3 cm/yr at E30, indicating net erosion at this site. Table 2 shows the significance of these results for $p > 0.05$. The remaining 19 stations cored in December 2000 are marked according to the criterion used to eliminate the station from further study. Stations marked '1' were not cored in at least two of the subsequent three cruises; those marked '2' had a December 2000 deposit thickness > 1 cm; those marked '3' lacked a visually clear contact in December 2000. Stations marked '4' passed these three criteria, but could not be analyzed as no common contact was found in the time series of images.

Table 2. ANOVA results testing significance of total thickness change shown in Figure 18.

Station	F_{data}	$F_{p>.05}$	Significant
D18	69.2	18.5	Yes
E11	231.0	9.6	Yes
E20	4.1	18.5	No
E25	1.2	9.6	No
E29	8.8	19.0	No
G15	246.0	9.3	Yes
H10	18.5	6.6	Yes
H18	4.1	9.6	No
J13	3.8	3.4	Yes
N14	4.7	9.6	No

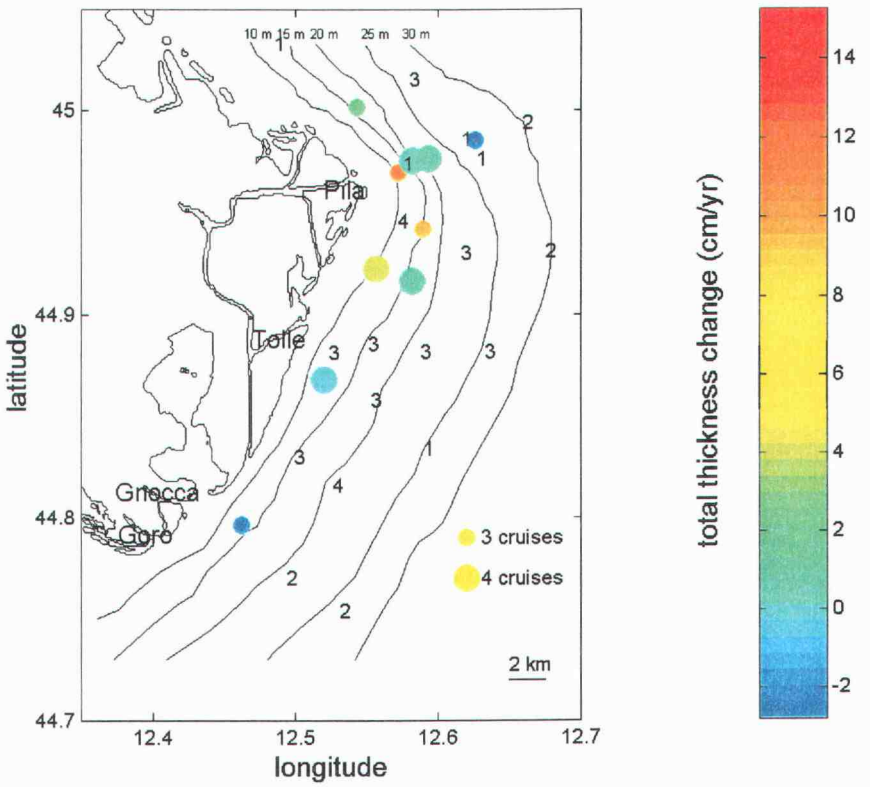

Figure 19. Averaged rate of total deposit thickness change between December 2000 and April 2002. Station spot size represents time over which marker layer was averaged; 3 cruises excludes April 2002 data. December 2000 stations not examined are marked numerically as: not cored in at least 2 of the subsequent three cruises (1); deposit thickness in December 2000 <1cm (2); December 2000 contact not clear visually (3); analysis attempted but no common contact was found (4)

Consolidation

Temporal consolidation measurements calculated from change in bed thickness within the deposit were only possible at three stations. Most beds used to estimate total thickness change had at least one edge blurred over more than 1 cm in both images for at least two of the coring times, thereby compromising this

method. Two layers at station H10 consolidated 5 % and 20 % (bulk density increase 0.08 g/cm^3 and 0.33 g/cm^3), and one layer in each of stations J13 and N14 consolidated 19 % and 12 % respectively (bulk density increase 0.31 g/cm^3 and 0.20 g/cm^3). If one assumes a porosity of 0.85 in December 2000, as was calculated from resistivity profiles at 0.25-mm intervals, available from the upper 10 cm of each box core (Table 3), then these bulk density increases would decrease porosity to 0.80, 0.65, 0.66, and 0.73, respectively.

Table 3. Summary of temporal porosity and consolidation change calculated from resistivity profiles at 0.25-mm intervals in the upper 10 cm of each box core throughout the four cruises (Archie's number = 2.4).

Cruise	Mean porosity	Mean density (g/cm^3)	Consolidation (%) (from Dec 00)	Porosity S.E.	n
Dec 00	.86	1.23		0.012	29
Jun 01	.73	1.45	13	0.012	24
Oct 01	.73	1.45	13	0.005	67
Apr 02	.76	1.40	10	0.018	23

Calculating the temporal change in bulk density based on changes in pixel brightness proved problematic. The conversion from brightness of a deposit bed to bulk density could not be made from the global equation due to an imager error present in many of the images, as well as variation in image exposure. Although variation in image exposure could be dealt with by creating a global equation for each of the exposure variations used, the presence of the imager error prevented use of any global equation. The imager error was found to occur in the majority of images, and to be image specific in the extent to which the brightness range was truncated (Figure 20). The imager error was due to an electronic component failure in the analogue to digital converter controlling output from the right side of the amorphous-silicon imager. The imager error was inconsistent across the image,

such that the target strip could not be used to calibrate brightness from within the same image (Note in Figure 20, the lower left and upper right panel of the target should have the same brightness).

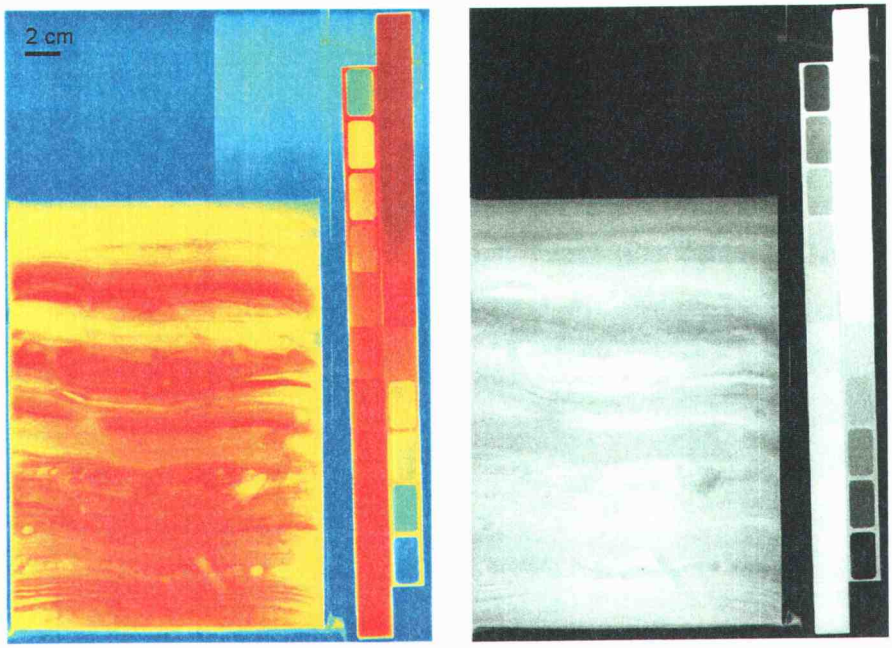

Figure 20. X-radiograph shown in pseudo-color with beam pattern removed to demonstrate the imager artifact. Note that the upper right and lower left target panel should be the same brightness

Small Scale Spatial Variability

The results of the nested ANOVA for flood layer thickness are shown in Tables 4 through 7. Table 4 and 5 show the three repeat cores at E16, and the two repeat cores at H10, have highly significant variance in thickness measurements made between image pairs within each core, and insignificant variance both between repeat cores at the station, and within measurements of each image. The four repeat cores at J13 were compared for both deposit thickness (Table 6) and depth to a silt layer visible in all images (Table 7). The silt layer depth, as with

replicate cores at E16 and H10, showed significant difference in measurements between pairs within a core, but not between cores or within images. The deposit thickness at J13 was the only result to find significant difference in thickness between repeats at a station (significant at 95 % confidence, not at 97.5 % confidence), variance was also significant between pairs within a core at J13.

Table 4. Nested ANOVA for flood layer thickness in three repeat cores taken at E16, October 2001

Source of variation	df	SS	MS	F_{data}	$F_{p>.05}$
Repeats w/in station	2	86.1	43.1	1.1	$F_{p>.05}[2,3]= 9.55$
Pairs w/in core	3	119.2	39.7	**102.3**	F.05[3,24]=3.01
Within image	24	9.3	0.4		
Total	29	214.6			
Variance partition	variance	%			
Repeats	0.3	3.9	cm		
Pairs	7.9	91.6	10s cm		
Image	0.4	4.5	10s m		
Sum	8.6				

Table 5. Nested ANOVA for flood layer thickness in two repeat cores taken at H10, April 2002

Source of variation	df	SS	MS	F_{data}	$F_{p>.05}$
Repeats w/in station	1.0	2.0	2.0	1.1	F.05[1,2]= 18.5
Pairs w/in core	2.0	3.6	1.8	**6.4**	F.05[2,16]=3.63
Within image	16.0	4.4	0.3		
Total	19.0	10.0			
Variance partition	variance	%			
Repeats	0.0	3.4	cm		
Pairs	0.3	50.2	10s cm		
Image	0.3	46.4	10s m		
Sum	0.6				

Table 6. Nested ANOVA for flood layer thickness in four repeat cores taken at J13, October 2001

Source of variation	df	SS	MS	F_{data}	$F_{p>.05}$
Repeats w/in station	3.0	86.9	29.0	**7.2**	F.05[3,4]= 6.59
Pairs w/in core	4.0	16.0	4.0	**11.8**	F.05[4,32]=2.68
Within image	32.0	10.9	0.3		
Total	39.0	113.8			
Variance partition	variance	%			
Repeats	2.5	69.9	cm		
Pairs	0.7	20.6	10s cm		
Image	0.3	9.5	10s m		
Sum	3.6				

Table 7. Nested ANOVA for silt layer depth in four repeat cores taken at J13, October 2001

Source of variation	df	SS	MS	F_{data}	$F_{p>.05}$
Repeats w/in station	3.0	3.7	1.2	1.3	F.05[3,4]= 6.59
Pairs w/in core	4.0	3.8	0.9	**6.1**	F.05[4,32]=2.68
Within image	32.0	4.9	0.2		
Total	39.0	12.4			
Variance partition	variance	%			
Repeats	0.0	8.5	cm		
Pairs	0.2	46.4	10s cm		
Image	0.2	45.1	10s m		
Sum	0.3				

DISCUSSION

The following discussion begins with an interpretation of the initial deposit thickness, contrasting the deposit to that seen on the Eel River margin, and addressing potential sampling error. The initial deposit thickness distribution is then used to calculate a deposit mass and compare the mass with expected sediment output from the Po River during the October 2000 flood. Next, the bulk density and edge contact methods are discussed with respect to testing on the Eel River data, and the two methods compared. In the deposit evolution section, the significance of small-scale spatial variability is discussed, followed by consolidation findings, and sources of issues relating to the conversion from brightness to bulk density. Consolidation is then removed from measurements of temporal thickness change to permit discussion of net erosion and deposition.

DETERMINING THE DEPOSIT THICKNESS

Initial Deposit Thickness

The October 2000 Po River flood deposit, as measured in December 2000, extends 7 km across the prodelta in water depths of 10-29 m. Maximum thickness is adjacent to the Pila mouth (10-25m), and near shore (< 15-m water depth) adjacent to the Tolle and Gnocca mouths. The deposit has a sharp thickness gradient, ranging from 38 cm to the deposit edge in approximately 7 km, and is confined to areas < 30-m water depth. Due to limitations set by the ship's draft, sampling was limited to ≥ 10-m water depth. Therefore, it is possible a large volume of flood sediment was deposited in < 10-m water depth; however, wave action may have prevented deposition within this region. Also, the initial deposit

analysis was confined to the areas cored in December 2000. This area excluded the region south of the Gnocca mouth, and adjacent to the Goro mouth, which together contribute to 24 % of the Po discharge (Nelson, 1970). This area was cored in subsequent cruises revealing deposit thickness up to 22 cm in 10-m water depth.

The spatial distribution of the Po flood deposit contrasts with observations by Wheatcroft and Borgeld (2000) of flood deposits on the Eel River margin. The Eel deposits were located entirely north of the river with the deposit centers of mass located 18 km from the river mouth, between the 50 and 100-m isobaths (Wheatcroft and Borgeld, 2000). In contrast, the Po deposit was concentrated adjacent to the Pila mouth, and extended a maximum of 9-km offshore to a depth of 30 m. The contrast in spatial distribution of the flood deposits can be explained by differences in the depositional environment. The Eel margin is a high energy environment, the discharge plume remained buoyant, and was carried north up the coast by strong wind-driven southerly currents (depth averaged current speed ~ 20 cm/s, Wheatcroft and Borgeld, 2000). Particle settling velocities of approximately 0.1cm/s (Hill et al., 2000) caused the plume to settle out 10 - 15 km north of the Eel mouth, followed by off-shore transport of the sediment as a density driven fluid mud flow within the wave boundary layer, to deliver sediment to the deposit site between the 50 and 100-m isobath (Traykovski et al., 2000). In contrast, the wind direction and speed and by implication currents at the Po mouth over the two month flooding period were variable (Figure 21), thus plume transport was limited. In addition, Po River sediment arrives at the sea in a flocculated state (pers. comm., P. Hill, 2002) thus it is more readily deposited proximal to the distributary mouths without significant resuspension. The deposition of sediment load immediately upon entering the sea is common in Mediterranean rivers (Nelson, 1972), perhaps due to high riverine nutrient levels allowing flocculation in lower salinity water (Milliman, 2001).

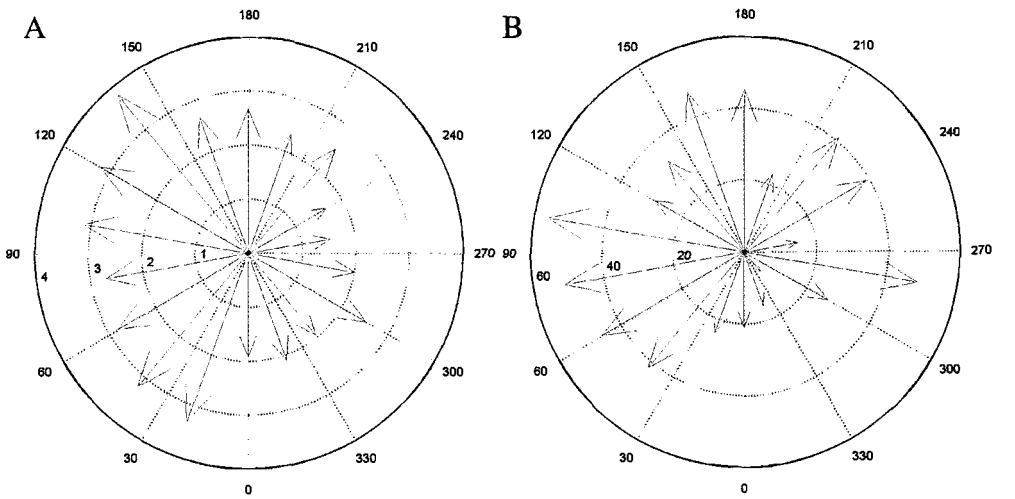

Figure 21. Directional wind data for October and November 2000, (A) wind speed (m/s), (B) number of 2 hr intervals with wind speed >1 m/s from the direction plotted. Source: ENEL Spa

Potential sources of error in measuring flood deposit thickness can be broken down into sampling error, imaging error, and image interpretation error. Imaging and interpretation errors are discussed in the following sections. Sampling error is meant to denote any biases that are introduced between coring and image collection. As a sample is taken compression of the sediment sample occurs at various stages. There is possibly loss of surficial sediments and compression of the entire boxed sample as the core penetrates the seabed (Blomqvist, 1991), then again as the box corer is placed on the ship's deck. As the x-radiography trays are pushed into the sediment additional compression occurs. Tray compression, measured in 30 subcores, averaged 5.3 % ± 0.6 % s.e. Once the sample is removed from the box core further compression may occur prior to imaging. Although the trays were typically x-rayed within one hour, some trays did sit overnight on the vibrating ship deck prior to imaging, consolidation was measured at 5 % in cores that sat 12 hours. Consolidation is more likely to occur in higher porosity sediment as there is more pore water to potentially remove (i.e., within the flood deposit). Total compression of a sample before being imaged is estimated at 5 – 10 %; hence

a measured flood deposit thickness of 15 cm can be estimated to have been roughly 16-cm thick in situ.

Deposit Mass

A starting point for obtaining a better understanding of flood sedimentation in general, and the Po River dispersal system in particular, is an estimate of the flood deposit mass. To calculate the deposit mass, thickness data were interpolated over the study area. The thickness data used were those calculated from the December 2000 images using the edge contact method (Figure 13) with the exceptions of J25 being set at 0-cm thick, D18 to 19-cm thick, and E11, E15, E20, and E25 to 36-cm, 36-cm, 32-cm, and 28-cm thick, respectively. These sites were adjusted to reflect the more likely deposit thickness at these stations as discussed in the edge contact section. In addition to these data, deposit thickness was measured from x-radiographs taken at stations off the Goro and Gnocca mouths in October 2001 that had not previously been cored, producing a more complete map of the deposit (Figure 22). Deposit thickness at one October 2001 station was difficult to assess due to bioturbation within the x-radiograph, as well as uncertainties as to possible contacts below the depth of core penetration (Figure 23), hence a thickness maximum and minimum estimate were used (Figure 22A and 22B), thus providing the range in calculations made below.

The deposit thickness data from each station were interpolated onto a 0.001-degree (approx. 93-m) grid spacing using a spline interpolation as described in Sandwell (1987). The spline interpolation provided tight constraint such that the thickness interpolation was retained within the area cored. The grid mean deposit thickness in > 10-m water depth was then calculated, and multiplied by the total grid area in > 10-m water depth (844 km^2) to yield a deposit volume (2.6 – 2.8 x

10^7 m^3). The December 2000 mean deposit porosity of 0.86 (Table 3) indicates 86 % of the deposit volume consists of pore-water, the remaining 14 % of sediment (3.6 – 4.0 x 10^6 m^3). The sediment volume was then multiplied by the assumed density of sediment grains (2.65 g/cm^3) to calculate the total deposit mass: 1.0 – 1.1 x 10^7 T.

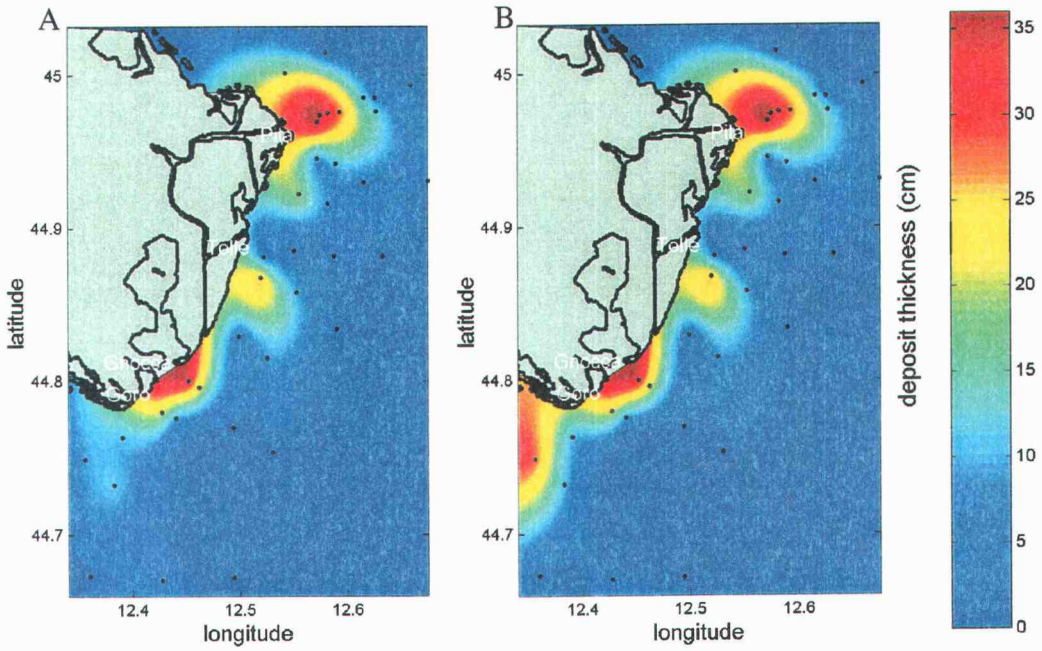

Figure 22. Estimated deposit thickness in December 2000, (A) minimum, (B) maximum

The flood sediment formed three depocenters adjacent to each of the river mouths. When spilt into three source mouths, 57 – 62 % of the deposit mass was located off the Pila mouth, 21 – 23 % off the Tolle, and 23 – 15 % off the Gnocca and Gorro. Nelson (1970) reports Po mouth sediment load partitioning for the Pila, Tolle, and Gnocca/ Goro at 74 %, 7 %, and 19 %, respectively of total sediment load discharge. It is possible that plume transport occurs to a small extent associated with the predominant southerly coastal current. Southerly transport

could explain the higher than expected deposit mass at the Tolle, Gnocca and Goro mouths.

Figure 23. X-radiograph from October 2001 in 10-m water depth adjacent to the Goro mouth (PQ10). Arrow marks depth of deepest edge contact detected. Deposit thickness uncertain due to bioturbation, and possible deeper contacts.

To estimate the percent of discharged sediment located within the deposit, an accurate estimate of the sediment load during the flood is needed. However, the estimate of sediment discharge by the Po is rough; no accurate estimate of flood sediment load for the Po exists in the literature aside from a 'maximum load' reported in Nelson (1970) which omits associated discharge information. According to Nelson (1970) monthly averaged sediment concentrations as high as 3,100 – 4,350 g/m^3 have been recorded during flooding of the Po, and December average sediment concentration was found to be 500 g/m^3. These concentrations are extremely high. Nevertheless, taking an estimate of average sediment

concentration between October 3 and December 2 of 2,100 g/m^3 ((3725 +500)/2) and applying it to the measured discharge, results in an estimated 5.5 x 10^7 T of sediment discharged by the Po during the October 2000 flood. If this figure were correct, then the total mass of sediment found in the deposit would represent approximately 20 % of the estimated total mass of sediment discharged. This figure is significantly lower than expected, as the near-mouth deposition pattern discussed above would presume minimal sediment escape from the study site. On the Eel River margin ~ 25 % of the sediment delivered to the ocean during floods was found to reside in a recognizable deposit (Wheatcroft and Borgeld, 2000). Due to the differences in deposit location relative to the source, and the much lower energy level, the percent of discharged sediment located within the Po deposit would be expected to greatly exceed this value. Assuming 50 %- 100% of the discharged sediment was within the deposit, the averaged sediment concentration over the 2 month flood period would have been 420 - 840 kg/m^3, a more realistic figure. Further effort in this area of research is warranted.

Bulk Density Method

The spatial distribution of stations where the bulk density method did not work is consistent with our expectations. Stations lacking a bimodal brightness distribution occur in two different sub-environments within the study area (Figure 12). The first sub-environment is on the seaward edge of the deposit; these stations are mostly in >25-m water depth and show minimal bulk density change within the image (stations marked '1' in Figure 12). Lack of bulk density change is expected at these stations as mean grain size typically decreases with depth. Finer grained sediment layers have a higher porosity, and hence lower bulk density, such that the bulk density of the pre-flood sediment at these deeper stations is likely to have been low, providing minimal bulk density contrast with the flood deposit. In addition,

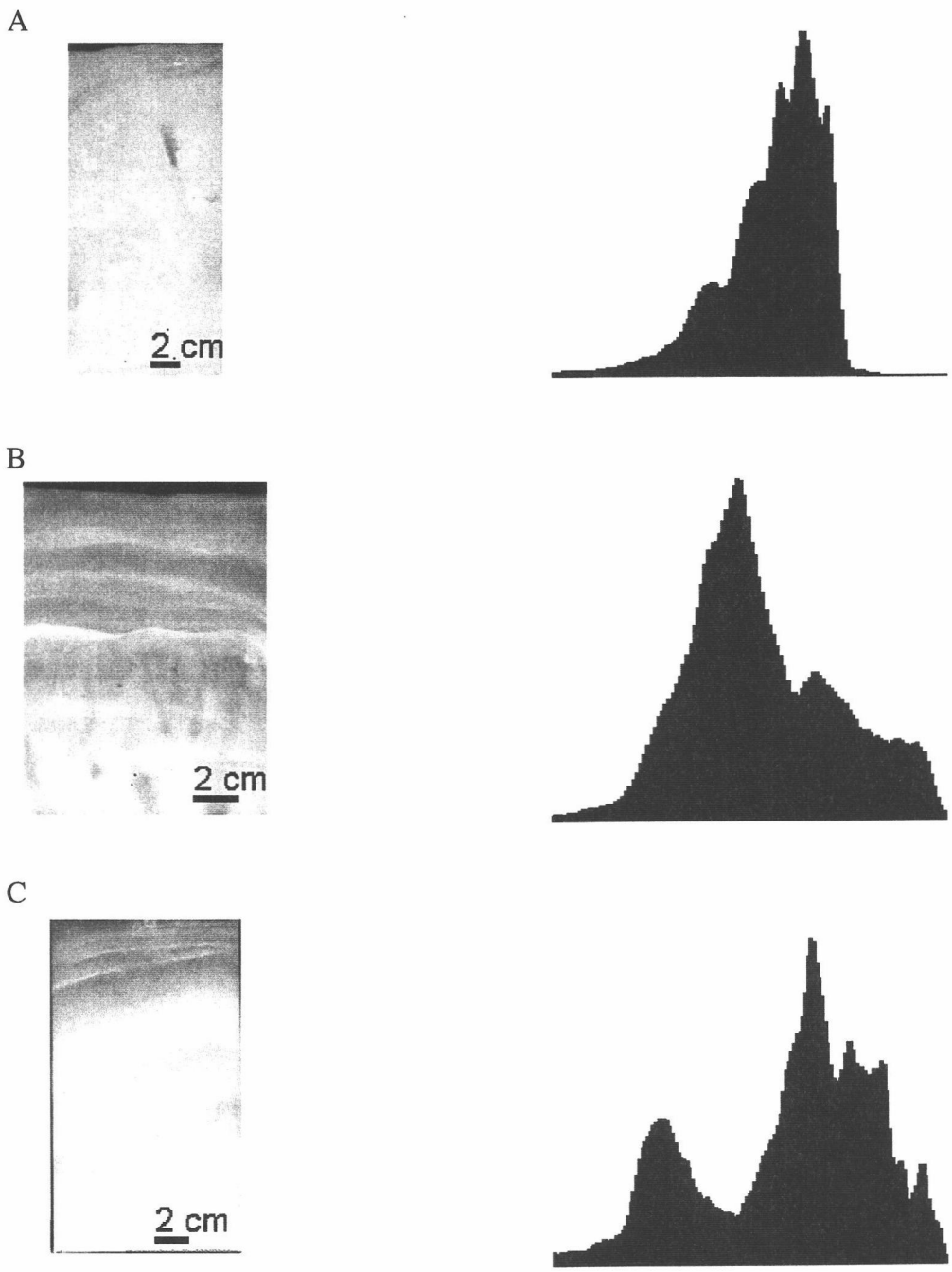

Figure 24 X-radiographs with brightness histograms showing non-bimodal distribution (x-axis runs from dark pixels (left) to light pixels (right)) for (A) I22 showing non-bimodal distribution due to deposit < 1-cm thick in 22-m water depth, (B) G10, showing uni-modal distribution due to bedding, and (C) H10, showing multi-modal distribution due to bedding

deposit thickness at these sites is generally <1 cm (as calculated from the edge contact method, Figure 13), hence the portion of image pixels having the lower bulk density associated with newly deposited sediment is not large enough to create a bimodal brightness distribution (Figure 24A).

The second sub-environment containing a concentration of stations with no bimodal brightness distribution is near the mouth of the Pila. These stations have the thickest flood deposit (as calculated from the edge contact method, Figure 13). It can be seen in Figure 13 that layering of differing bulk density bands within the flood deposit is most prevalent at sites containing thick flood deposits. Therefore, the deposits at stations near the Pila mouth would be expected to have internal bedding, and hence no bimodal brightness distribution. Layering of dense silt bands within the deposit results in a non-bimodal brightness distribution, as a large range of sediment density occurs within the deposit (Figure 24B and 24C).

Edge Contact Method

This method enabled an estimate of flood deposit thickness to be made from every image. Stations with images containing layering of differing bulk density bands (marked '2' in Figure 13) all had flood deposits > 10-cm thick, and layering was present in all stations with > 12-cm deposit. These stations with bedding are concentrated on the E line, proximal to the Pila mouth, or near the other mouths in < 15-m water depth. At these stations the measurement based on the edge contact method represents a minimum deposit thickness as the method gives no indication of the likelihood of additional contacts occurring below the core depth (generally < 40 cm). Even with the deeper images, available from kasten cores, this method had to be combined with the texture map for an accurate deposit thickness measurement of stations with internal bedding within the flood deposit.

The edge contact method can produce apparently erroneous estimates of deposit thickness at sites where older, buried contacts are present, or where the basal contact is blurred. The problem of older deposits became evident in the Eel data comparison where previous work had indicated presence of old deposits (Sommerfield et al., 2002) – which were indeed detected using the edge contact method. Texture maps confirmed that only one Po station, J25, had a sub-deposit contact, possibly created by benthic infauna (Figure 15). Contact blurring was a problem at only one station in the December 2000 images; D18 had a blurred basal contact at 19 cm, hence a silt layer at 12 cm was detected as the deposit base (Figure 25). Both stations D18 and J25 had non bimodal brightness distributions, and texture maps showed no texture change across the incorrectly selected contact.

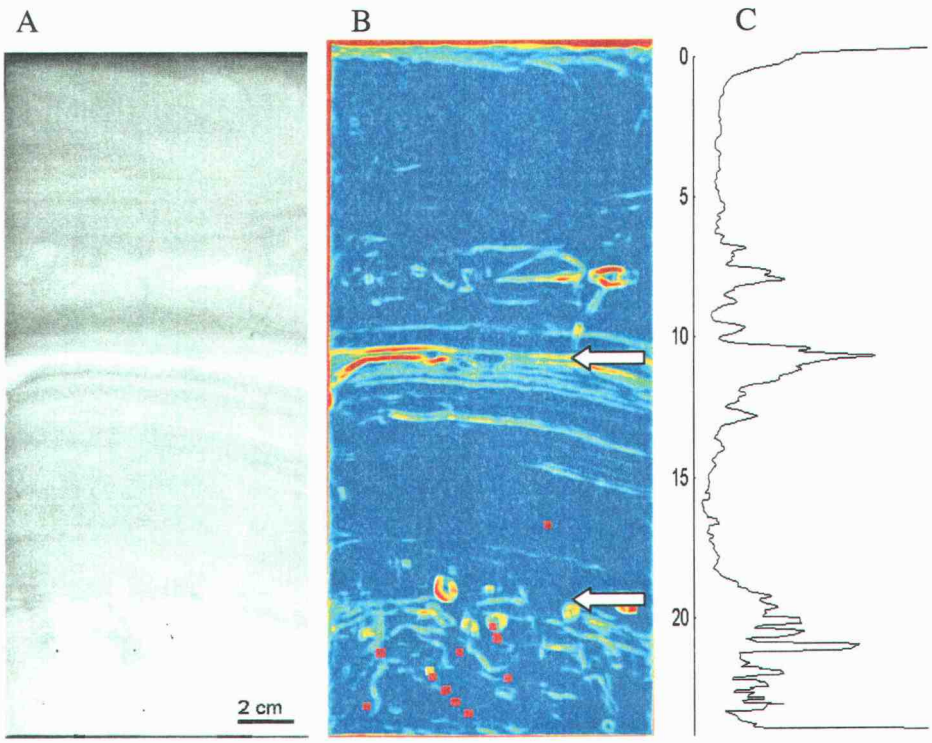

Figure 25 (A) an example image from D18 showing use of the texture map (B) to determine correct deposit depth at base of bedding (top arrow shows deepest contact depth, lower arrow shows marked texture change, see text), (C) row average plot of the texture map with scale bar in cm.

As images were compared over subsequent cruises for deposit evolution measurements, the reference horizons used became less distinguishable in the edge maps from the later cruises. Therefore, this method is most reliable when applied to newly deposited sediments containing minimal bedding within the deposit.

Eel River Comparison

The two objective methods developed herein showed disagreement with the Wheatcroft and Borgeld (2000) results at only four of twenty seven stations investigated on the Eel margin. However, to highlight potential shortcomings of the objective methods, each of these mismatches will be discussed in detail. Station L70 in February 1995 was reported as having 4-cm deposit thickness by Wheatcroft and Borgeld (2000), but only a 1.3-cm thickness with both objective methods used herein (Figure 26A). The true basal contact was not detected by the edge contact method as several sections of the contact are blurred by what appears to be biological reworking. Given the relatively thin bed and the five week lag between the flood and coring, such reworking is not surprising (Figure 26A). The bulk density method did not detect the deeper section of the deposit, as between 1.3-cm and 4-cm depth the deposit is closer in bulk density to the sediment below than to the sediment overlying the silt layer at 1.3 cm. Only one image from L70 was analyzed, hence the method errors could not be detected by mismatch from another image from the box core.

The three sites showing disagreement in the January 1997 comparison were O70, Q70, and U70. O70 is another site where the objective techniques could be applied to just one image. Both methods detect the deposit base at 1.6 cm when the actual deposit base is more likely at 4.3 cm - the depth given by Wheatcroft and Borgeld (2000) based on multiple independent techniques (Figure 26B).

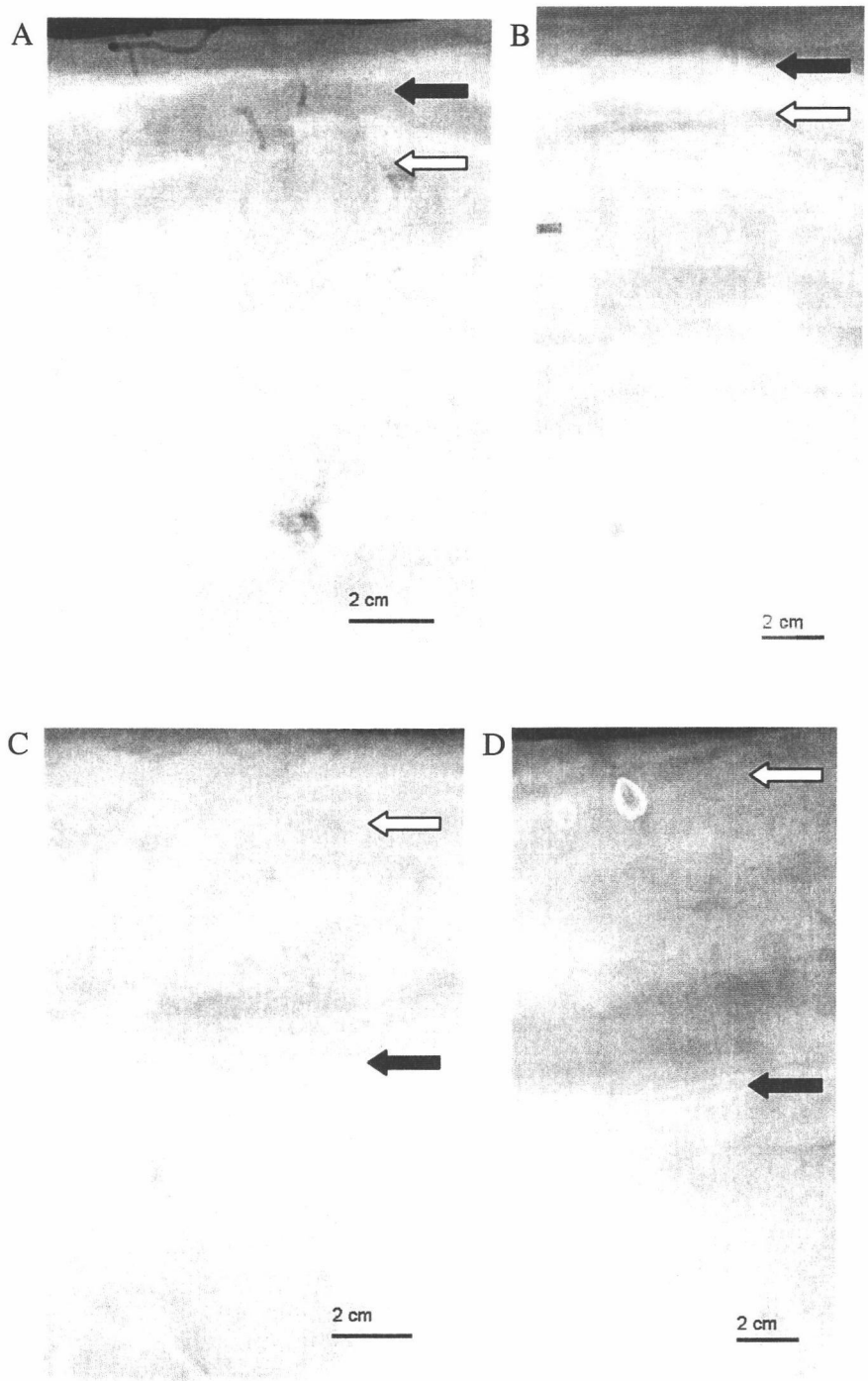

Figure 26. Images from the Eel River flood deposit, (A) L70, 1995; (B) O70, 1997; (C) Q70, 1997; (D) U70, 1997. Arrows indicate depths referred to in the text with respect to erroneous

thickness measurements, white = Wheatcroft and Borgeld depths, black = objective method depths.

The deposit between the depth of 1.6 and 4.3 cm is a thick silt layer. The edge contact method misses the deposit base as the brightness change is minimal and blurred, and the bulk density method misses the base as the silt layer is more dense than most of the underlying sediment. Q70 is reported as having a 3.1-cm deposit by Wheatcroft and Borgeld (2000), however, both images from this site show a deeper contact at 9 cm that was picked up by both objective methods as being the deposit base (Figure 26C). Earlier flood deposits on the Eel margin have been recognized (Wheatcroft and Drake, 2003). The contact at 9 cm was not picked up in the March 1995 analysis as the image from Q70 in March 1995 only extended 8-cm deep. The same situation applies at U70 where a clear contact exists at 11.3 cm but the thickness reported by Wheatcroft and Borgeld (2000) is 1.2 cm (Figure 26D). Again this deeper contact was not seen in the shorter March 1995 image. In the Po analysis, station J25 was the only site determined as having a contact deeper than the flood deposit thickness. A thick (>1.5 cm) silt layer is not evident at the deposit base in any of the Po images. The agreement in the two objective methods with each other and the Wheatcroft and Borgeld (2000) data (Figure 17) confirms the ability of the imaging techniques to detect the flood deposit thickness accurately.

Objective Method Comparison

The bulk density method and the edge contact method predict deposit thickness with a close 1:1 relationship (0.99 correlation coefficient for 56 images). Both methods yield similar thickness results, but have problems with the following two image types: when banding is present within the deposit, and when sub-

deposit or blurred contacts exist. Banding is better analyzed using the edge contact method, and basal contact blurring or sub deposit contacts are better resolved using the bulk density method. The edge contact method provides a depth for every image analyzed, compared to only 41 % of images having bimodal brightness distribution. However, the use of both methods provides a more accurate and objective determination of deposit thickness for any given image.

The development of these two methods has provided a quantitative, objective means of incorporating the advantages of x-radiography into a sediment analysis tool. The integration of the two methods provides accurate analysis, more quantitative in application than methods previously used.

DEPOSIT EVOLUTION

Small-Scale Spatial Variability Significance

The results of the nested ANOVA show that variance on tens-of-meter scales (between repeat cores) is insignificant, hence it can be expected that when a station is re-cored on subsequent cruises, the significant changes seen in deposit thickness are truly differences in deposit thickness, rather than small-scale spatial variability.

Significant variance was seen to occur on the tens-of-centimeter scale (between image pairs within a core), possibly due to physical deposition structures such as ripples (e.g., Goff et al., 2002) as was noted within deposit bands of some images with wavelengths and amplitudes of several centimeters (e.g., at E11 were variance between imager pairs is highest). It is also possible that methodological

variability such as box coring artifacts previously discussed could contribute variability at this within-core scale.

Consolidation

Measurements of consolidation based on a decrease in bed thickness were difficult to assess due to the rarity of layers that persisted through April 2002 with distinct upper and lower contacts. Most beds used to estimate temporal bulk density increase had at least one edge blurred, or an edge that changed brightness over more than 1 cm in both images for at least two of the coring times. Contacts meeting the requirement were only found at three stations (H10, J13, N14). However, the consolidation of those layers (mean consolidation 13.8 % ± 3.5 s.e. n=4) is within the range of values indicated by time-series porosity measurements calculated from resistivity profiles in the upper 10 cm of each box core throughout the four cruises (Table 3).

Estimates of consolidation based on temporal changes in brightness would be a useful method of estimating deposit consolidation were it not for the imager artifact. The imager artifact that was present in the majority of the images used in this study has since been fixed therefore should not prove a problem in further studies. Despite this improvement, there are many issues that need to be addressed to fully realize the technique, and these are discussed next.

Non-uniform irradiance of the sample due to x-ray beam pattern was removed using a global beam pattern map. This beam pattern image could be shot as a set-up procedure at the beginning of each cruise to ensure predictability not only of the beam pattern, but of imager problems that may have arisen since last use. Ideally a single calibration target should be used throughout the study. The

ceramic target was not used after December 2000; however, both the aluminum and glass targets were used on the following cruises. X-ray attenuation is predominantly dependent on the volumetric electron density of the substance, but it is also slightly dependent on the atomic number of the attenuating material as described in the x-radiography section. Therefore the AL should also be discontinued from use. The difference in absorption coefficients between aluminum and silicon are such that a 1.5 g/cm^3, 22-mm thick sample shot at 75 kV would result in the aluminum bar appearing to be 0.12 g/cm^3 less dense than the glass bar.

Sample thickness is also critically important. Calibration targets are all created on 28-mm thick strips (the nominal thickness of a sample tray including the front and back face plate) and the known density of each bin is calculated over 22 mm to allow for the exclusion of the 3 mm front and back face of the tray from the sediment density conversion calculation. The inner thickness of a tray is 22 mm (Figure 4), but as it is inserted into the box core, bowing of the front plate often occurs. Observations of bowing were made on earlier cruises, and measurements of tray bowing were made on the April 2002 cruise. Of 31 trays measured, 20 had bowing >1 mm. Of those 20 trays, 16 bowed outwards, resulting in a thicker sample, and 4 bowed inwards, resulting in a thinner sample. The maximum bow was 5 mm out and 3 mm in, the mean of those trays bowing out was 2.4 mm and of those bowing in was 2 mm. An imaged tray with sediment bow of 5 mm out from the 22-mm expected thickness adds 0.34 g/cm^3 of bulk density error, which correlates to an apparent porosity decrease of 20 % (thickness increase of (22+5)/22 = 1.23, mean sediment bulk density = 1.5 g/m^3, bulk density increase = (1.5 x 1.23) – 1.5 = 0.34 g/m^3). This error could be removed in the future either by measuring the bow in each sample and having a bow dependant correction factor, or by constructing new trays of a more rigid material. Differing sample trays were also used throughout the four cruises. Variance in polycarbonate type and

thickness may have created slight x-ray absorption and scattering differences, as well as variance in tray widths responding differently to bowing effects. Each of the above mentioned issues, imager error, global beam pattern, multiple calibration targets, core bowing, and core size and material inconsistencies, either has, or can in hindsight be averted in future studies.

The consolidation results show expected patterns. The high consolidation rate between December 2000 and June 2001 (Table 3) is expected as newly deposited sediment with high porosity consolidates. Subsequent deposition and thus burial of the bed also occurred at most sites during this time (Figure 18). Mean bulk density is unchanged between June 2001 and October 2001, then decreases slightly by April 2002. The decrease in bulk density could be associated with benthic infauna increasing porosity through burrowing (Hanor and Marshall, 1971), working against the increase in bulk density caused by temporal consolidation.

An implication of these results is the 'apparent erosion' caused by consolidation. A consolidation factor of 10 – 13 % (see Table 3) needs to be removed from measurements of total thickness change before erosion and deposition rates can be inferred from the total thickness change measurements made.

Erosion and deposition

Processes at the sediment surface (i.e., deposition and erosion), as well as internal processes (i.e., consolidation) combine to change total bed thickness over time. To consider net deposition and erosion at the study site, total thickness values were adjusted to correct for consolidation effect (Figures 27 and 28).

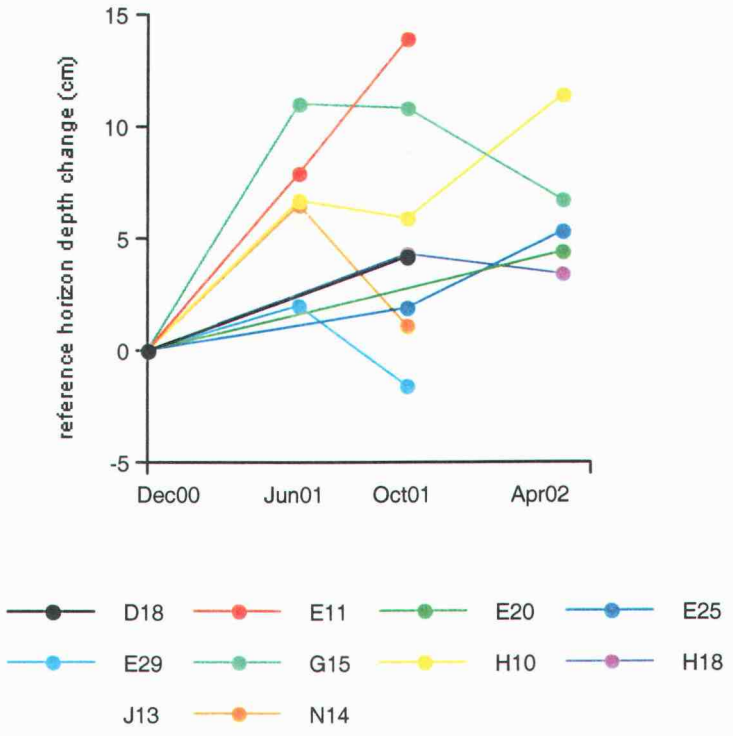

Figure 27. Net deposition (consolidation removed) between December 2000 and April 2002. Note thickness is not necessarily the deposit thickness, as in some cases a silt layer was used to trace deposit thickness change. Error bars indicate s.e. between images at each station (n = 2-8)

The apparent erosion seen at station E29 and N14 in Figure 19 is due to bed consolidation, as in Figure 28 both these sites have < 2 cm/yr total thickness change. Continued deposition was seen at all sites between December 2000 and June 2001 (Figure 27). At E11 deposition continued throughout the sampling period until April 2002 at an average rate of 15 cm/yr.

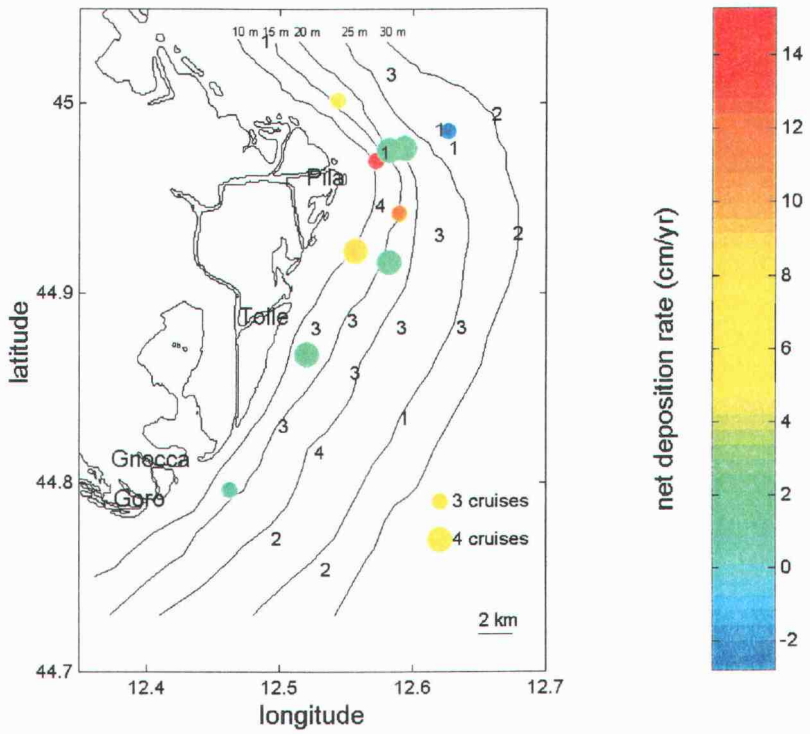

Figure 28. Averaged rate of net deposition (consolidation removed) between December 2000 and April 2002. Station spot size represents time over which marker layer was averaged, and December 2000 stations not examined are marked numerically as in Figure 18.

The absence of significant erosion at the study site is expected given the generally low energy environment of the northern Adriatic. Hourly orbital wave velocities measured at 1 m above the sediment/water interface at 12-m water depth exceeded 20 cm/s only 18 days of 305 sampled, and exceeded 30 cm/s only once (sampled January 27 – June 3 2001, October 14 2001 – April 10 2002) (pers. comm., A. Fain, University of Washington). These velocities indicate that even at the shallower stations bottom stresses are generally sub-critical (mean orbital wave velocity 3 cm/s).

CONCLUSIONS

The two methods developed for measuring flood deposit thickness (edge contact method and bulk density method) have provided a quantitative, objective means of incorporating the advantages of x-radiography into a sediment analysis tool. The integration of the two methods provides analysis of sedimentary structures without the subjectiveness of previous methods.

The initial flood deposit distribution is concentrated near the Pila mouth in shallow-water stations, where up to 38 cm (at 11-m water depth, E11) of deposition occurred. The cross-shore deposit thickness gradient is sharp with the deposit edge at <30-m depth, <9 km off the Pila mouth. Along-shore variation in deposit thickness is varied; deposit thickness is high (> 15 cm) at nearshore (10-m depth) stations proximal to river mouths and low (7 cm) at other nearshore stations. This distribution is likely a result of the low energy environment that allowed immediate deposition of Po River sediment load with little dispersal or subsequent resuspension.

The deposit mass as mapped was calculated at approximately 10^7 T. 60 % of this mass is located adjacent to the Pila mouth, approximately 14 % less than predicted from sediment load partitioning between mouths as reported by Nelson (1970), suggesting possible southerly transport of the flood plume toward the Tolle, Gnocca, and Goro mouths, where proportionally more sediment was seen than expected. An estimate of the percent of total sediment discharge during the October 2000 flood located within the deposit was difficult to make due to the lack of accurate sediment load estimates during flooding. Assuming 50 – 100% of the total flood sediment load is located within the deposit, the mean sediment concentration during the flood can be estimated at 420 – 840 kg/m^3.

Continued deposition between December 2000 and April 2002 occurred at sites proximal to the Pila mouth at rates up to 15 cm/yr (at station E11). Significant erosion did not occur at any station between December 2000 and April 2000; consistent with the generally low velocity bottom currents measured at a benthic tripod. Consolidation of the deposit between December 2000 and April 2002 averaged 10 %, with the majority of the consolidation occurring by June 2001.

FURTHER APPLICATION

The digital x-radiography system used, combined with the objective image analysis techniques developed in this research, allows for future comprehensive, efficient study of flood deposits by incorporating the advantages of x-radiography into a quantitative, objective sediment analysis tool. Future applications of the approach will also benefit from the incorporation of recommendations listed in the discussion for avoiding imaging difficulties.

The system used could be applied to numerous fields of sedimentary study, ranging from bedding formation and bioturbation studies, to disturbance studies (i.e. storm or trawling effects). Information such as biological structure abundance, and recolonization by benthic infauna, could be obtained from a data set such as this were the comparison of images less complicated by imaging issues encountered on this first field testing of the digital x-radiography system.

REFERENCES

Ambrogi R., Bedulli D., and Zurlini G. (1990) Spatial and temporal patterns in structures of macrobenthic assemblages. A three-year study in the northern Adriatic Sea in front of the Po River delta. *Marine Ecology* 11: 25-41

Axelsson V. (1983) The use of X-ray radiographic methods in studying sedimentary properties and rates of sediment accumulation. *Hydrobiologia* 103: 65-69

Axelsson V. (1994) X-ray radiographic techniques in studying sedimentary properties, sedimentary sequences, and rates of sedimentation: A manual. http://home.swipnet.se/valter/manual2.htm

Barmawidjaja D. M., van der Zwaan G. J., Jorissen F. J., and Puskaric S. (1995) 150 years of eutrophication in the northern Adriatic Sea: Evidence from a benthic foraminiferal record. *Marine Geology* 122:367-384

Blomqvist S. (1991) Quantitative sampling of soft bottom sediments: problems and solutions. *Marine Ecology Progress Series* 72: 295-304

Boldrin A., Bortoluzzi G., Frascai F., Guerzoni S., and Rabitti S. (1988) Recent deposits and suspended sediments off the Po Della Pila (Po River main mouth), Italy. *Marine Geology* 79: 159-170

Bondesan M. (1990) L'area deltizia padana: caratteri geografici e geomorfologici. In *"Il Parco dei delta del Po: studi ed immagini, vol. II"* 10-48. http://www.regione.emilia-romagna.it/geologia/econv_pia.htm

Bouma, A. H. (1964) Notes on x-ray interpretation of marine sediments. *Marine Geology* 2: 278-309

Briggs K. B., Jackson P. D., Holyer R. J., Flint R. C., Sandidge J. C., and Young D. K. (1998) Two-dimensional variability in porosity, density, and electrical resistivity of Eckernforde Bay sediment. *Continental Shelf Research* 18: 1939-1964

Brush G. S., Martin E. A., Defries R. S., and Rice C. A. (1982) Comparisons of ^{210}Pb and pollen methods for determining rates of estuarine sediment accumulation, Potomac Estuary. *Quaternary Research* 18: 196-217

Catteneo A., Correggiari A., Langone L., and Trincardi F. (in review) Late Holocene garagano subauquous delta, Adriatic shelf: sediment pathways and supply fluctuations. *Journal of sedimentary research*

Colantoni P., Gallignani P., and Lenaz R. (1979) Late Pleistocene and Holocene evolution of the north Adriatic continental shelf. *Marine Geology* 33: M41-M50

Dott Jr R.H. (1982) SEPM presidential address: Episodic sedimentation - how normal is average? How rare is rare? Does it matter? *Journal of Sedimentary Petrology* 53: 5-23

Edmondson W.T. (1991) Sedimentary record of changes in the condition of Lake Washington. *Limnology & Oceanography* 36: 1031-1044

Envirtech. http://www.envirtech.org. 37 Via XX Settembre, 16121 Genoa, Italy.

Feng H., Cochran J. K., Hirschberg D. J., and Wilson R.E. (1998) Small-scale spatial variations of natural radionuclide and trace metal distributions in sediments from the Hudson River estuary. *Estuaries* 21: 263-280

Grimm K. A., Lange C. B., and Gill A. S. (1996) Biological forcing of hemipelagic sedimentary laminae: evidence from ODP Site 893, Santa Barbara Basin, California. *Journal of Sedimentary Research A: Sedimentary Petrology & Processes* 66: 613-624

Goff J.A., Wheatcroft R.A., Lee H., Drake D.E., Swift D.J.P., and Fan S. (2002) Spatial variability of shelf sediments in the STRATAFORM natural laboratory, northern California. *Continental Shelf Research* 22: 1199-1223

Hamblin K. (1962) X-ray radiography in the study of structures in homogeneous sediments. *Journal of sedimentary petrology* 32: 201 – 210

Hanor J. S., and Marshall N. F. (1971) Mixing of sediment by organisms. Trace Fossils, A field guide to selected localities in Pennsylvanian, Permian, Cretaceous and Tertiary rocks of Texas and related papers. Perkins, B.F. [ed.] S. E. P. M. 127-135

Hill P. S., Milligan T. G., and Geyer W. G. (2000) Controls on effective settling velocity of suspended sediment in the Eel River flood plume. *Continental Shelf Research* 20: 2095-2111

Howard J. D. (1968) X-ray radiography for examination of burrowing in sediments by marine invertebrates. Sedimentology 11: 249-258

Hoyler R. J., Young D.K., Sandidge J. C., and Briggs K. B. (1996) Sediment density structure derived from texture analysis of cross-sectional x-radiographs. *Geo-Marine Letters* 16: 204-211

Kourafalou V. H. (1999) Process studies on the Po River plume, northern Adriatic Sea. *Journal of Geophysical Research* 104: 29,963 29,985

Kuehl S. A., Pacioni T. D., and Rine J. M. (1995) Seabed dynamics of the inner Amazon continental shelf: temporal and spatial variability of surficial strata. *Marine Geology* 125: 283-302

Leithold E. L. (1989) Depositional processes on an ancient and modern muddy shelf, northern California. *Sedimentology* 36: 179-202

Milliman J. D. (2001) Delivery and fate of fluvial water and sediment to the sea: a marine geologist's view of European rivers. *Scientia Marina* 65: 121-132

Milliman J. D., and Meade, R. H. (1983) World-wide delivery of river sediment to the oceans. *The Journal of Geology.* 91: 1-21

Mulder T., Migeon S., Savoye B., and Faugeres J. C. (2001) Inversely graded turbidite sequences in the deep Mediterranean: a record of deposits from flood-generated turbidity currents? *Geo-Marine Letters* 21: 86-93

Nelson B. W. (1970) Hydrography, sediment dispersal, and recent historical development of the Po River delta, Italy. Deltaic Sedimentation Modern and Ancient. *Tulsa, Oklahoma, Society of Economic Paleontologists and Mineralogists.* J. P. Morgan and R.H. Shaver [Eds]. 152 - 184.

Nelson, B. W. (1972). Mineralogical Differentiation of Sediments Dispersed from the Po delta. *The Mediterranean Sea: A Natural Sedimentation Laboratory.* 441-453.

Nittrouer C. A., and Sternberg R. W. (1981) The formation of sedimentary strata in an allochthonous shelf environment: the Washington continental shelf. *Marine Geology* 42: 201-232

Orsi T. H., Edwards C. M., and Anderson A. L. (1994) X-ray computed tomography: A nondestructive method for quantitative analysis of sediment

cores. *Journal of Sedimentary Research A: Sedimentary Petrology & Processes* A64: 665-703

Pemberton, S. G., and MacEachern J. A. (1997) The ichnological signature of storm deposits: the use of trace fossils in event stratigraphy. *Paleontological events: stratigraphic, ecological, and evolutionary implications.* Brett, Carlton E., Baird, Gordon C. [Eds]. Columbia University Press. New York & Chichester. 73-109

Russ J. C., (1995) *The image processing handbook.* Second edn. CRC press

Santschi P. H., Cappellino S., Dobbs C., McShea L., Allison M. A., Asbill S., and Perlet A. B. (1999) Sediment transport and HG recovery in Lavaca Bay, as evaluated from radionuclide and HG distributions. *Environmental Science and Technology* 33: 378-391

Sandwell D. T. (1987) Biharmonic spline interpolation of GEOS-3 and SEASAT altimeter data. *Geophysical Research Letters* 14: 139-142

Sekulić B., and Vertačnik A. (1996) Balance of average annual fresh water inflow into the Adriatic Sea. *Water Resources Development* 12: 89-97

Smith C. R., McMurtry G., Gage J. D., Levin L. A., and Hoover D. J. (2000) Variations in bioturbation across the oxygen minimum zone in the northwest Arabian Sea. *Deep-Sea Research Part II: Topical Studies in Oceanography* 47: 227-257

Sokal R. R., and Rohlf F. J. (1981) Biometry. Second edn., Freeman

Sommerfield C. K., Drake D. E., and Wheatcroft R. A. (2002) Shelf record of climatic changes in flood magnitude and frequency, north-coastal California. *Geology* 30:395-398

Sommerfield C. K., Nittrouer C. A., and Alexander C. R. (1999) ^{7}Be as a tracer of flood sedimentation on the northern California continental margin. *Continental Shelf Research* 19:335-361

Traykovski P., Geyer W. R., Irish J. D., and Lynch J. F. (2000) The role of wave-induced density-driven fluid mud flows for cross-self transport on the Eel River continental shelf. *Continental Shelf Research* 20: 2113-2140

Van Straaten L. M. J. U. (1965) Sedimentation in the north western part of the Adriatic Sea. *Submarine geology and geophysics: proceedings of the seventeenth symposuim of the Colston Research Society*. 143-160

Wetzel A., and Aigner T. (1986) Stratigraphic completeness: tiered trace fossils provide a measuring stick. *Geology* 14: 234-237

Wheatcroft R. A. (2000) Oceanic flood sedimentation: A new perspective. *Continental Shelf Research* 20: 2059-2294

Wheatcroft R. A., and Borgeld J. C. (2000) Oceanic flood deposits on the northern California shelf: Large-scale distribution and small-scale physical properties. *Continental Shelf Research* 20: 2163-2190

Wheatcroft R. A., and Drake D. E. (2003) Post-depositional alteration and preservation of sedimentary event layers on continental margins, I. The role of episodic sedimentation. *Marine Geology*, submitted

Wheatcroft R. A., Borgeld J. C., Born R. S., Drake D. E., Leithold E. L., Nittrouer C. A., and Sommerfield C. K. (1996) The anatomy of an oceanic flood deposit. *Oceanography* 9: 158-162

APPENDICES

APPENDIX A

Table A Thickness measurements made on each December 2000 image. Standard deviation (Std) of the 5 evenly spaced thickness measurements within each image.

Image Name	Bulk Density Method		Edge Contact Method	
	Thickness (cm)	Std	Thickness (cm)	Std
P1_B16LA	0.9	0.3	1.1	0.6
P1_B16NA	1.1	0.1	1.0	0.1
P1_D18LA			12.0	0.2
P1_D18NA			12.1	0.3
P1_D28LA	3.9	0.4	3.5	0.7
P1_D28NA	4.0	0.7	3.1	0.2
P1_E11LA			27.0	
P1_E11NA			26.4	
P1_E15LA			22.9	
P1_E15NA			22.9	
P1_E20LA			22.9	
P1_E20NA			22.9	
P1_E25LA			12.3	0.6
P1_E25NA	13.1	0.5	13.8	0.5
P1_E28TA	13.0	1.6	12.3	1.8
P1_E28WA	12.6	0.4	11.4	0.7
P1_E29NA	8.0	1.1	7.2	1.2
P1_E30NA			0.0	
P1_F29NA	12.0	1.8	12.4	2.3
P1_F29WA			11.4	0.9
P1_G10LA	11.8	0.3	12.1	0.6
P1_G10NA			6.3	0.2
P1_G15LA			10.3	0.4
P1_G15NA			10.6	0.4
P1_G23LA			6.5	1.1
P1_G23NA	5.1	0.1	5.8	0.2
P1_G29NA			0.0	
P1_G29WA			0.9	0.1
P1_H10NA			17.4	0.6
P1_H10WA			18.0	0.2
P1_H18TA			8.1	0.3
P1_H18WA	7.0	0.5	8.1	0.2
P1_I10NA	7.3	0.3	7.9	

P1_I10WA	5.6	1.1	6.4	1.7
P1_I17NA	1.3	0.2	1.2	0.3
P1_I17WA			1.5	
P1_I22NA				
P1_I22WA	1.6	0.6	2.1	0.2
P1_I26NA			1.3	0.1
P1_I26WA			1.2	0.3
P1_J13LA	20.9	0.5	21.8	0.2
P1_J13TA	24.5	0.8	24.5	0.7
P1_J20NA	7.5	0.5	8.6	0.3
P1_J20NB	10.0	0.6	9.9	0.4
P1_J25LA			0.0	0.0
P1_J25NA			10.1	0.7
P1_L16NA	5.7	0.7	6.0	1.1
P1_L16WA			5.6	0.8
P1_L21TA			6.6	0.1
P1_L21WA			9.8	0.6
P1_N14TA	22.4	0.5	22.2	0.4
P1_N14WA			21.1	1.0
P1_N22			0.0	0.0
P1_N22WA			0.0	0.0
P1_N25LA			0.0	0.0
P1_N25NA			0.0	0.0
P1_Q21LA			3.5	0.4
P1_Q21NA			0.0	0.0
P1_Q25LA			0.0	0.0
P1_Q25NA			0.0	0.0
P1_S25LA			1.3	0.3
P1_S25NA			1.6	0.3
P1_U25LA	3.3	0.2	0.0	0.0
P1_U25N			0.9	0.4
P1_U25NA			1.1	0.6

APPENDIX B

Table B Box core locations of images used in this study. Stations listed more than once represent replicate cores.

Station	Dec-00		Jun-01		Oct-01		Apr-02	
(degrees)	Lat.	Long.	Lat.	Long.	Lat.	Long.	Lat.	Long.
B16	45.0325	12.4854						
D18	45.0015	12.5429			45.0012	12.5431	45.0013	12.5434
D28	45.0150	12.5796	45.0145	12.5794	45.0145	12.5803	45.0150	12.5790
E11	44.9695	12.5717	44.9694	12.5716	44.9693	12.5720	44.9687	12.5724
E15	44.9738	12.5753						
E16a					44.9737	12.5757		
E16b					44.9736	12.5755		
E16c					44.9737	12.5759		
E20	44.9756	12.5817	44.9757	12.5818	44.9755	12.5815	44.9753	12.5822
E25	44.9762	12.5928	44.9764	12.5938	44.9761	12.5929	44.9757	12.5932
E28	44.9857	12.6157					44.9853	12.6154
E29	44.9855	12.6262	44.9853	12.6270	44.9854	12.6264		
E30	44.9939	12.6590	44.9937	12.6599			44.9935	12.6594
F29	44.9765	12.6265						
G10	44.9458	12.5725	44.9449	12.5718	44.9459	12.5722	44.9454	12.5728
G15	44.9422	12.5894	44.9415	12.5888	44.9419	12.5893	44.9413	12.5890
G23	44.9299	12.6160	44.9303	12.6164	44.9297	12.6159	44.9294	12.6159
G29	44.9308	12.6745						
H10a	44.9225	12.5558	44.9224	12.5556	44.9223	12.5557	44.9222	12.5559
H10b							44.9224	12.5563
H18	44.9163	12.5818	44.9164	12.5824	44.9157	12.5816	44.9162	12.5821
I10	44.8811	12.5226	44.8817	12.5226	44.8811	12.5229	44.8792	12.5236
I17	44.8854	12.5515	44.8856	12.5516	44.8850	12.5508	44.8852	12.5514
I22	44.8816	12.5884	44.8807	12.5882	44.8815	12.5879	44.8806	12.5879
I26	44.8815	12.6326	44.8820	12.6325	44.8815	12.6327		
J13a	44.8674	12.5203	44.8674	12.5203	44.8670	12.5202	44.8676	12.5209
J13b					44.8675	12.5203		
J13c					44.8673	12.5204		
J13d					44.8673	12.5199		
J20	44.8578	12.5529	44.8581	12.5528	44.8574	12.5535	44.8573	12.5528
J25	44.8339	12.5899			44.8342	12.5898		
L16	44.8294	12.4995	44.8294	12.5000	44.8294	12.5000	44.8298	12.4997
L21	44.8156	12.5265	44.8158	12.5265	44.8156	12.5265	44.8155	12.5259
N10					44.8000	12.4524		

N14	44.7963	12.4616	44.7958	12.4615	44.7963	12.4616	44.7956	12.4606
N22	44.7698	12.4936	44.7699	12.4934	44.7690	12.4939	44.7694	12.4931
N25	44.7535	12.5315			44.7536	12.5312	44.7535	12.5309
O10					44.7800	12.4267		
O14					44.7760	12.4413		
P10					44.7627	12.3907		
P15					44.7531	12.4099		
PQ10					44.7485	12.3563		
PQ15					44.7316	12.3832		
Q15					44.6732	12.3599		
Q21	44.6705	12.4268	44.6712	12.4256	44.6701	12.4268	44.6703	12.4262
Q25	44.6721	12.4940			44.6721	12.4937		
S25	44.5881	12.5094						
U25	44.5047	12.5144						

APPENDIX C

Table C Replicate core measurements. Depths 1 – 5 are the 5 evenly spaced thickness measurements within each image. Image mean thickness and box mean thickness are also given. A, B, C, and D are replicate cores. s, w, n, and e are different x-radiographs from within a single core.

E16 Oct01	depth 1	depth 2	depth 3	depth 4	depth 5	image mean	box mean
As	21.6	22.0	22.4	22.6	22.6	22.2	22.5
Aw	22.8	22.4	22.2	22.7	23.8	22.8	
Bs	22.1	21.3	20.8	20.6	20.0	20.9	21.2
Bw	20.5	21.1	21.2	21.5	22.5	21.4	
Cs	28.2	28.3	28.7	28.4	29.8	28.7	25.2
Cw	22.2	21.7	22.1	21.7	21.4	21.8	
H10 Apr02							
An	14.5	14.2	13.8	14.1	14.5	14.2	14.6
Ae	13.8	14.3	14.8	15.7	16.0	14.9	
Bn	15.0	14.6	14.8	14.7	14.6	14.7	15.2
Bs	15.1	15.4	15.4	15.3	14.4	15.1	
Be	15.3	15.3	15.6	16.2	16.0	15.7	
Bw	14.9	14.7	15.8	15.6	15.6	15.3	
J13 silt Oct01							
As	11.9	11.4	11.4	11.6	12.3	11.7	11.5
Aw	11.6	11.2	11.4	10.9	11.3	11.3	
Bs	13.3	12.4	12.6	12.9	12.3	12.7	12.2
Bw	12.6	11.9	11.9	11.5	11.2	11.8	
Cs	11.5	11.5	11.3	11.2	11.3	11.4	11.7
Cw	11.7	11.5	11.9	12.8	12.4	12.0	
Ds	11.6	11.2	11.4	10.9	12.1	11.5	11.5
Dw	11.9	11.6	11.6	11.1	11.6	11.6	
J13 Oct01							
As	26.1	25.1	25.6	26.4	27.7	26.2	26.8
Aw	27.0	27.1	27.3	27.3	28.1	27.4	
Bs	24.6	23.6	24.1	24.2	23.5	24.0	23.5
Bw	23.3	23.3	23.0	23.0	22.6	23.0	
Cs	21.6	22.5	23.0	23.0	23.5	22.7	23.2
Cw	23.3	23.5	23.8	23.8	24.0	23.7	
Ds	23.8	24.5	24.6	24.1	24.3	24.3	23.4
Dw	23.2	22.9	23.0	21.6	21.8	22.5	